Princeton Plasma Physics Laboratory

PPPL- 4487

PPPL- 4487

Whistler Wave Excitation and Effects of Self-Focusing on Ion Beam Propagation through a Background Plasma along a Solenoidal Magnetic Field

Mikhail A. Dorf, Igor D. Kaganovich, Edward A. Startsev, and Ronald C. Davidson

February, 2010

PPPL PRINCETON PLASMA PHYSICS LABORATORY

Prepared for the U.S. Department of Energy under Contract DE-AC02-09CH11466.

Princeton Plasma Physics Laboratory
Report Disclaimers

Full Legal Disclaimer

Trademark Disclaimer

PPPL Report Availability

Princeton Plasma Physics Laboratory:

http://www.pppl.gov/techreports.cfm

Office of Scientific and Technical Information (OSTI):

http://www.osti.gov/bridge

Related Links:

U.S. Department of Energy

Office of Scientific and Technical Information

Fusion Links

Whistler Wave Excitation and Effects of Self-Focusing on Ion Beam Propagation through a Background Plasma along a Solenoidal Magnetic Field

Mikhail A. Dorf, Igor D. Kaganovich, Edward A. Startsev, and Ronald C. Davidson
Plasma Physics Laboratory, Princeton, New Jersey, 08543

This paper extends studies of ion beam transport through a background plasma along a solenoidal magnetic field [I. Kaganovich *et al*., Phys. Plasmas **15**, 103108 (2008)] to the important regime of moderate magnetic field strength satisfying $\omega_{ce} > 2\beta_b\omega_{pe}$. Here, ω_{ce} and ω_{pe} are the electron cyclotron frequency and electron plasma frequency, respectively, and $\beta_b = v_b/c$ is the directed ion beam velocity normalized to the speed of light. The electromagnetic field perturbations excited by the ion beam pulse in this regime are calculated analytically, and verified by comparison with the numerical simulations. The degrees of beam charge neutralization and current neutralization are estimated, and the transverse component of the Lorentz force associated with the excited electromagnetic field is calculated. It is found that the plasma response to the ion beam pulse is significantly different depending on whether the value of the solenoidal magnetic field is below or above the threshold value specified by $\omega_{ce}^{cr} = 2\beta_b\omega_{pe}$, and corresponding to the resonant excitation of large-amplitude whistler waves. The use of intense whistler wave excitations for diagnostic purposes is also discussed.

I. INTRODUCTION

Neutralization and focusing of a charged particle beam by a background plasma form the basis for a variety of applications to high energy accelerators and colliders[1,2], ion-beam-driven high energy density physics and fusion[3,4], and astrophysics[5,6]. For instance, one of the modern approaches to ion beam compression for heavy ion fusion applications is to use a dense background plasma which charge neutralizes the ion charge bunch, and hence facilitates compression of the bunch against strong space-charge forces[3-4,7-8]. Additional control and focusing of the beam pulse can be provided by the application of a solenoidal magnetic field in the neutralizing region[9,10,11,12,13]. It has recently been demonstrated that even a weak magnetic field can significantly change the degrees of charge neutralization and current neutralization of an ion beam propagating through a background plasma[14-15]. In Refs. [14, 15] detailed analysis of an ion

beam propagating through a neutralizing plasma background along a solenoidal magnetic field has been performed for the regime of a weak applied magnetic field satisfying $\omega_{ce} < 2\beta_b\omega_{pe}$, where ω_{ce} and ω_{pe} are the electron cyclotron and plasma frequencies, respectively, and $\beta_b = v_b/c$ is the directed ion beam velocity normalized to the speed of light *c*. In this paper, we extend earlier studies of nonrelativistic beam neutralization to the case where $\omega_{ce} > 2\beta_b\omega_{pe}$. An important difference between the two regimes appears to be due to excitation of electromagnetic wave-field perturbations, which propagate oblique to the beam axis for the case where the applied magnetic field exceeds the threshold value corresponding to $\omega_{ce}^{cr} = 2\beta_b\omega_{pe}$. Therefore, the slice approximation previously used for the analysis of the case where $\omega_{ce} < 2\beta_b\omega_{pe}$ in Refs. [14, 15], and not taking into account the effects of coupling between the longitudinal and transverse dynamics cannot, in general, be applied in the present studies, and a different approach has to be developed. Note that the threshold value of the magnetic field can be expressed as $B_c = 2\beta_b\left(n_p\left[cm^{-3}\right]/10^{11}\right)^{1/2} kG$. For instance, for an ion beam with $\beta_b \sim 0.05$ propagating through a background plasma with density n_p~10^{11} cm^{-3}, this corresponds to a relatively weak magnetic field of 100 G.

In the present analysis, we consider a fast ion beam pulse with velocity much greater than the Alfven velocity, and therefore the beam ions cannot interact effectively with ion Alfven wave excitations. Furthermore, we assume a smooth beam density profile with a characteristic axial length scale for density variation, l_b, much greater than the wavelength of electron plasma wave excitations, $l_b >> v_b/\omega_{pe}$. Therefore, electrostatic electron plasma wave excitations are also significantly suppressed[16-17]. However, if a sufficiently strong ambient magnetic field with $\omega_{ce} > 2\beta_b\omega_{pe}$ is present inside the neutralizing region, the ion beam pulse can effectively interact with the electromagnetic electron whistler branch of the plasma dispersion relation[18-19]. Therefore, in the present paper we analyze excitation of the whistler branch by an ion beam pulse propagating through a neutralizing plasma along a solenoidal magnetic field, and assess its influence on the degrees of beam charge neutralization and current neutralization, and the transverse beam dynamics.

The fundamental problem of whistler wave-field perturbations excited by a charged particle beam propagating in a magnetized plasma has been extensively studied for several

decades, and various methods have been developed[19,20,21,22,23,24]. Recent interest in this problem has been motivated by possible use of charged particle beams for space communications. Propagating in the magnetized ionosphere or the magnetosphere plasma, charged particle beams can excite whistler wave-field perturbations, and therefore can be used as compact on-board emitters in the very-low-frequency range, replacing large-apertures electromagnetic antennas[19-21]. Analytical and numerical studies of whistler branch excitations by a density-modulated electron beam propagating through a background plasma along a uniform magnetic field, including both linear and nonlinear effects have been reported in Refs. [22-24]. However, in those calculations the case of a thin beam with $r_b << k_\perp^{-1}$ has been considered, and the effects of the transverse beam structure have not been taken into account. Here, r_b is the characteristic beam radius, and $k_\perp$ is the perpendicular component of the whistler wave vector. Note that in contrast to space-physics phenomena, where the wavelength of the whistler waves is large compared to the beam radius, for the parameters typical of neutralized intense ion beam transport applications, the beam radius can be comparable to the perpendicular wavelength. Furthermore, an axially-continuous, density-modulated beam with modulation period l_m has been considered in Refs. [22-24], and therefore a monochromatic wave excitation with frequency $\omega = v_b / l_m$ was obtained. Note that a finite-length ion beam pulse with a bell-shaped (not modulated) axial density profile used in intense beam transport applications can excite a broad frequency spectrum with a characteristic frequency $\omega \sim v_b / l_b$ and bandwidth $\delta\omega \sim \omega$. Therefore, in the present analysis we consider excitation of the electromagnetic whistler branch by a finite-length ion beam pulse propagating through a background plasma along a solenidal magnetic field, taking into account the effects of the longitudinal and transverse beam structures.

In the present paper we demonstrate that the total electromagnetic field excited by the ion beam pulse can be conveniently represented as the sum of two components: a *local* field component, corresponding to the local polarization of the background plasma, and rapidly decaying to zero outside the beam pulse; and a *wave* field component that can extend far outside the beam. It is then shown that in the regime where $\omega_{ce} >> 2\beta_b \omega_{pe}$ the local-field component has the dominant influence on the transverse beam dynamics. Moreover, in this limit, a positive charge of the ion beam pulse becomes over-compensated by the plasma electrons, resulting in an enhanced transverse focusing of the beam ions. Note that for the case where $\omega_{ce} < 2\beta_b \omega_{pe}$

considered in Refs. [14, 15], the beam charge is under-neutralized, and the radial electric field has a defocusing effect. Furthermore, it is shown that the local plasma response is changing from paramagnetic for the $\omega_{ce} < 2\beta_b\omega_{pe}$ case [14, 15], to diamagnetic for the $\omega_{ce} > 2\beta_b\omega_{pe}$ case. The threshold value of the magnetic field $\omega_{ce}^{cr} = 2\beta_b\omega_{pe}$, which separates these qualitatively different regimes of ion beam interaction with the background plasma, corresponds to the resonant excitation of a large-amplitude wave-field component [22].

It is important to point out that the effects of resonant wave excitation can be utilized for diagnostic purposes. Indeed, placing a pick-up loop outside the beam pulse and varying the amplitude of the applied magnetic field, a large-amplitude signal will be detected when the applied magnetic field approaches the threshold value specified by $\omega_{ce}^{cr} = 2\beta_b\omega_{pe}$. Therefore, it is expected that this scheme can be utilized as a passive diagnostic tool to measure the beam velocity or plasma density.

This paper is organized as follows. The theoretical model and assumptions in the present analysis are described Sec. II. In Sec. III we consider the regime of resonant wave excitation, present the asymptotic time-dependent solution in the linear approximation, and estimate the saturation amplitude due to the nonlinear response of the plasma electrons. The analytical solutions for the electromagnetic field are compared to the results of numerical particle-in-cell simulations in Sec. IV. Finally, in Sec. V a detailed analysis of the local field excitations, including the effects of enhanced beam self-focusing, is presented.

II. THEORETICAL MODEL

In this section we calculate the electromagnetic field excitation generated by an ion beam pulse propagating through a cold background plasma with a constant velocity, v_b, along a uniform magnetic field $\mathbf{B}_{ext} = B_{ext}\hat{z}$. The beam carries a current of $j_b = Z_b e n_b(z - v_b t, x)$, where Z_b is the beam ion charge state, $-e$ is the electron charge, n_b is the beam number density, and x and z are the transverse and longitudinal coordinates, respectively. For simplicity in the analytical studies, we consider here 2D slab (x,z) geometry, and the results of numerical simulations in cylindrical (r,z) geometry are presented in Sec. IV. Provided the beam density is small compared to the plasma density ($n_b << n_p$), we assume a linear (small-signal) plasma response and obtain the following

equation for the Fourier transforms of the perturbed electromagnetic field components $\mathbf{E} = \int d\mathbf{k} d\omega \mathbf{E}_{\omega,\mathbf{k}} \exp(-i\omega t + ik_x x + ik_z z)$ and $\mathbf{B} = \int d\mathbf{k} d\omega \mathbf{B}_{\omega,\mathbf{k}} \exp(-i\omega t + ik_x x + ik_z z)$ [25]:

$$k^2 \mathbf{E}_{\omega,\mathbf{k}} - \mathbf{k}(\mathbf{k} \cdot \mathbf{E}_{\omega,\mathbf{k}}) - \frac{\omega^2}{c^2} \vec{\varepsilon} \cdot \mathbf{E}_{\omega,\mathbf{k}} = \frac{4\pi i}{c} \mathbf{j}_{\omega,\mathbf{k}} . \quad (1)$$

Here, $\vec{\varepsilon}$ is the dielectric tensor describing linear response of the cold plasma electrons[25] with $\varepsilon_{xx} = \varepsilon_{yy} = 1 - \omega_{pe}^2 / (\omega^2 - \omega_{ce}^2)$, $\varepsilon_{zz} = 1 - \omega_{pe}^2 / \omega^2$, and $\varepsilon_{xy} = -\varepsilon_{yx} = i\omega_{pe}^2 \omega_{ce} / [\omega(\omega^2 - \omega_{ce}^2)]$, where $\omega_{pe} = (4\pi e^2 n_p / m_e)^{1/2}$ is the plasma frequency, $\omega_{ce} = eB_{ext} / m_e c$ is the electron cyclotron frequency, and the plasma ion response is neglected provided $k_x l_b << \sqrt{m_i / m_e}$ [26]. Here, m_e and m_i are the electron mass and ion mass, respectively. Finally, we neglected perturbations in the ion beam motion, assuming that the time duration of beam-plasma interaction is smaller than the characteristic time for the ion beam response [26]. The space-time Fourier transform of the beam current is specified by $\mathbf{j}_{\omega,\mathbf{k}} = Z_b e n_{\mathbf{k}}(k_z, k_x) \delta(\omega - k_z v)$, where $n_{\mathbf{k}} = \int d\xi dx n_b(\xi, x) \exp(-ik_x x - ik_z \xi)$.

It is straightforward to show for this model of the beam current that Eq. (1) yields a steady-state solution, in which all quantities depend on z and t solely through the combination $\xi = z - v_b t$. In what follows, we assume that the beam pulse is sufficiently long, with $r_b << l_b$ and $\omega \sim v_b / l_b << \omega_{pe}$. Note that the latter condition implies that electrostatic electron plasma wave excitations are significantly suppressed[16-17]. Finally, in this section, for simplicity we assume that $\omega_{ce} << \omega_{pe}$, and a general analysis for the case of an arbitrary ratio of $\omega_{ce} / \omega_{pe}$ can be found in Appendix A. For present purposes, it is particularly important to analyze the x-component of the electric field perturbations, E_x, and the y-component of the magnetic field perturbations, B_y, which determine the transverse dynamics of the beam particles. After some straightforward algebra we obtain the following Fourier transforms of the transverse electromagnetic field components

$$\frac{eE^x_{\omega,\mathbf{k}}}{m_e \omega_{pe} c} = -i \frac{c^3 Z_b k_x k^2 \omega_{ce}^2}{n_p \omega_{pe} (\omega_{pe}^2 + c^2 k^2)^2} \frac{k_z^2 v_b^2 n_{\mathbf{k}} \delta(\omega - k_z v_b)}{\omega^2 - \omega_{wh}^2(k_x, k_z)} , \quad (2)$$

$$\frac{eB^y_{\omega,\mathbf{k}}}{m_e \omega_{pe} c} = -i \frac{\beta_b Z_b \omega_{pe} c k_x}{n_p (\omega_{pe}^2 + c^2 k^2)} \frac{k_z^2 v_b^2 n_{\mathbf{k}} \delta(\omega - k_z v_b)}{\omega^2 - \omega_{wh}^2(k_x, k_z)} , \quad (3)$$

where use has been made of Faraday's equation, $(\omega/c)\mathbf{B}_{\omega,\mathbf{k}} = \mathbf{k}\times\mathbf{E}$, to obtain the perturbed magnetic field component. Here, $\beta_b = v_b/c$, $k^2 = k_x^2 + k_z^2$, and

$$\omega_{wh}^2(k_x,k_z) = \frac{\omega_{ce}^2 k^2 k_z^2}{\left(k^2 + \omega_{pe}^2/c^2\right)^2}, \tag{4}$$

is the dispersion relation for the electron whistler branch. The electromagnetic field perturbations E_x and B_y, can now be obtained by applying inverse space-time Fourier transforms to Eqs. (2) and (3). Integration over the frequency ω readily gives

$$\frac{eE_{\mathbf{k}}^x}{m_e\omega_{pe}c} = -i\frac{c^3 Z_b k_x k^2 \omega_{ce}^2}{n_p\omega_{pe}\left(\omega_{pe}^2 + c^2k^2\right)^2}\frac{k_z^2 v_b^2 n_{\mathbf{k}}\exp(-ik_z vt)}{k_z^2v^2 - \omega_{wh}^2(k_x,k_z)}, \tag{5}$$

$$\frac{eB_{\mathbf{k}}^y}{m_e\omega_{pe}c} = -i\frac{\beta Z_b \omega_{pe} c k_x}{n_p\left(\omega_{pe}^2 + c^2k^2\right)}\frac{k_z^2 v_b^2 n_{\mathbf{k}}\exp(-ik_z vt)}{k_z^2v^2 - \omega_{wh}^2(k_x,k_z)}. \tag{6}$$

It is evident that the onset of wave-field generation by the beam pulse corresponds to existence of real solutions to

$$\omega_{wh}^2(k_x,k_z) = k_z^2 v_b^2. \tag{7}$$

Note that the condition in Eq. (7) is equivalent to the resonance condition for Cherenkov radiation, namely $V_z^{ph} = v_b$, where V_z^{ph} is the z-component of the whistler wave phase velocity.

(a) Properties of the excited whistler waves

It is straightforward to show that real solutions to Eq. (7) exist, provided

$$\alpha = \omega_{ce}/2\beta_b\omega_{pe} > 1, \tag{8}$$

as illustrated in Fig. 1(a). For this case, the solutions $k^2 = k_{em,qs}^2$ correspond to the long-wavelength electromagnetic part of the whistler branch, $k = k_{em} < \omega_{pe}/c$, and the short-wavelength quasi-electrostatic part, $k = k_{qs} > \omega_{pe}/c$ [Fig. 1(a)]. In the limit where $\alpha >> 1$ the solutions are approximately given by

$$k_{qs} \cong \frac{2\alpha\omega_{pe}}{c},\ k_{em} \cong \frac{\omega_{pe}}{2\alpha c}. \tag{9}$$

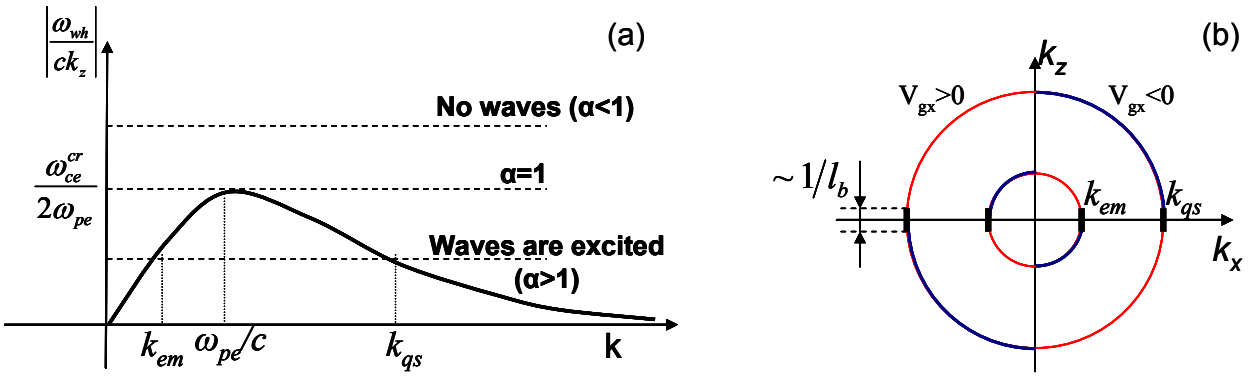

Fig. 1. Plots of solutions to Eq. (7) corresponding to the wave vectors of the excited whistler wave-field. (a) The absolute value of the normalized z-component of the whistler wave phase velocity (solid curve) is intersected by different values of the normalized beam velocity β_b (dashed lines). (b) The circles on the plane (k_x,k_z) illustrate the solutions to Eq. (7). For the case of a long beam pulse with $l_b >> k_{qs,w}^{-1}$, the wave vectors primarily excited are illustrated by the short vertical bold lines. Red and blue colors illustrate positive and negative signs, respectively, of the x-component of the group velocity for the excited waves.

Note that for a long beam pulse with $k_z^{-1} \sim l_b >> k_{qs,em}^{-1}$ the transverse wave vectors of the excited wave field are approximately given by $k_x \approx \pm k_{qs,em}$ [see Fig. 1(b)].

The directions of the x-component of the group velocity V_{gx} for the excited wave field are illustrated in Fig. 1(b). Note that the quasi-electrostatic and the long-wavelength electromagnetic whistler waves with the same signs of phase velocity have opposite signs of group velocity, V_{gx}. Furthermore, it can be shown that the z-component of the group velocity for the short-wavelength quasi-electrostatic wave field is smaller than the beam velocity. In contrast, the long-wavelength electromagnetic wave field propagates in the z-direction faster than the beam. *Therefore, the long-wavelength electromagnetic perturbations excited by the beam tail can propagate along the beam and influence the dynamics of the beam head.* A schematic illustration of the whistler wave excitations is shown in Fig. 2.

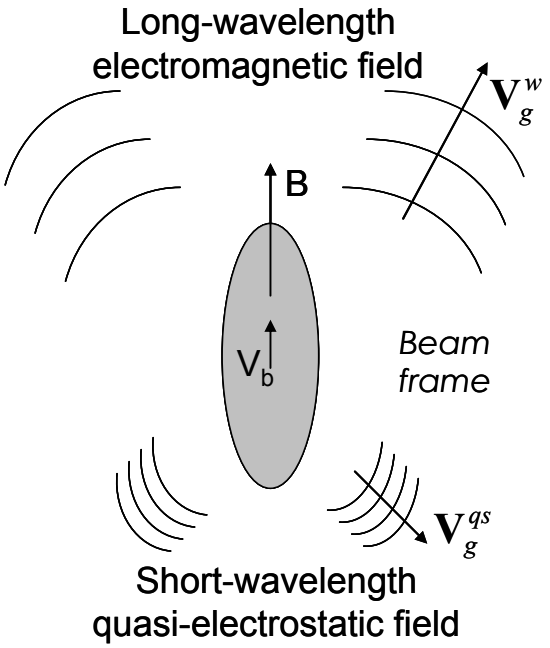

Fig. 2. Schematic illustration of the whistler waves excited by the ion beam pulse. In the beam frame of reference, the long-wavelength electromagnetic wave-field propagates ahead of the beam pulse, and the short-wavelength quasi-electrostatic wave-field propagates toward the beam tail.

(b) Wave-field and local-field components of the excited electromagnetic perturbations

Wave-field excitations for the case where $\alpha > 1$ are associated with the poles in Eqs. (5)-(6), which appear in the real space of the wave vector components (k_x,k_z). Note, for the case of a long beam pulse, $k_z^{-1} \sim l_b >> k_{qs,em}^{-1}$, that the pole locations on the real k_x-axis depend weakly on the value of k_z, $k_x \cong \pm k_{em,qs}\left(1 + k_z^2 / 2k_{em,qs}^2\right)$. It is therefore convenient to carry out the inverse Fourier integration, first along the k_x-axis, and then along the k_z-axis. To properly account for the pole contributions, the integration over k_x-space should be carried out along the Landau contour, C_L, as illustrated in Fig 3. Note that integration along the contour C_L shows that sufficiently far outside the beam only wave fields with a positive (negative) x-component of group velocity propagate in the region $x>0$ ($x<0$).

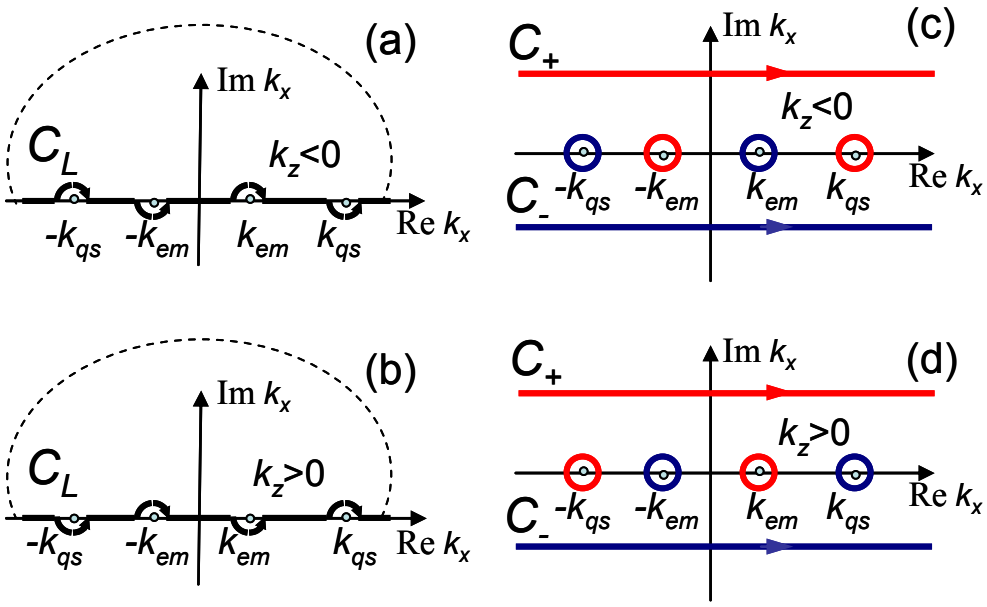

Fig. 3. Integration contours used for evaluation of the integrals in Eqs. (4)-(5). Frames (a) and (b) show Landau contours C_L corresponding to $k_z<0$ and $k_z>0$, respectively. Frames (c) and (d) illustrate contours of integration equivalent to the ones shown in Frames (a) and (b), respectively. Red and blue colors are used to illustrate the integration contours for $x>0$ and $x<0$, respectively.

To demonstrate this fact, as an illustrative example, we consider the simple case where the spectrum of the beam density is an analytical function in the complex k_x-plane, which satisfies $n_{\mathbf{k}} \exp(-|k_x x|) \to 0$ for large values of $|k_x|$. Considering $x>0$, and closing the Landau contour through a semi-circle of an infinitely large radius lying in the upper-plane [Figs. 3(a) and 3(b)], we readily obtain that the wave field excitations correspond to contributions from the poles at $k_x=-k_{em}$ and $k_x=k_{qs}$ for $k_z<0$, and at $k_x=k_{em}$ and $k_x=-k_{qs}$ for $k_z>0$. Note that the group velocity of these waves is indeed directed away from the beam, i.e., $V_{gx}>0$ [see. Fig. 1(b)]. Finally, it should be pointed out that the integration contours C_L are different for the cases where $k_z>0$ and $k_z<0$. Therefore, even for a symmetric longitudinal beam density profile, the electromagnetic field perturbations are not, in general, symmetric around the beam center, implying oblique wave propagation.

For present purposes, it is convenient to represent the integration along the contour C_L for $x>0$ ($x<0$) as an integral along a slightly shifted upward (downward) contour C_+ (C_-) lying below

(above) the poles of $n_{\mathbf{k}}$, plus (minus) the residues of the relevant on-axis poles [Figs. 3(c) and 3(d)]. For a beam with a smooth radial profile it can be shown that the contribution from the on-axis poles corresponds to the wave-field components of the electromagnetic field perturbation (E_x^W, B_y^W) extending far outside the beam, and the integral along the path C_+ corresponds to the local-field components (E_x^{loc}, B_y^{loc}) that rapidly decays to zero outside the beam. Assuming $k_z << k_{em,qs}$ for a sufficiently long beam pulse, we obtain the following approximate expressions for the wave-field components of the electromagnetic field perturbation for $x>0$,

$$\frac{eB_y^W}{m_e\omega_{pe}c} = \frac{2\pi\omega_{pe}\beta_b Z_b}{cn_p\left(k_{qs}^2 - k_{em}^2\right)}\left(b_{em} + b_{qs}\right), \tag{10}$$

$$\frac{eE_x^W}{m_e\omega_{pe}c} = \frac{2\pi Z_b\omega_{ce}^2}{cn_p\omega_{pe}\left(k_{qs}^2 - k_{em}^2\right)}\left(e_{em} + e_{qs}\right). \tag{11}$$

Here,

$$b_{qs,em} = \pm\left(k_{qs,em}^2 + \omega_{pe}^2/c^2\right)\int_0^\infty dk_z n_{\mathbf{k}}\left(k_{qs,em}, k_z\right)\cos\left[k_z\xi \mp k_{qs,em}\left(1 + k_z^2/2k_{qs,em}^2\right)x\right], \tag{12}$$

$$e_{qs,em} = \pm k_{qs,em}^2\int_0^\infty dk_z n_{\mathbf{k}}\left(k_{qs,em}, k_z\right)\cos\left[k_z\xi \mp k_{qs,em}\left(1 + k_z^2/2k_{qs,em}^2\right)x\right], \tag{13}$$

are the electric and magnetic components corresponding to the quasi-electrostatic (with subscript "*qs*") and the long-wavelength electromagnetic (with subscript "*em*") waves, respectively, and $\xi = z - v_b t$. Note that the correction term, $\delta\varphi = \left(k_z^2/2k_{em,qs}\right)x$, which we only retained in the phase of the wave-field component, yields a curvature in the phase fronts, and a corresponding decrease in the wave-field amplitude for $x \geq l_b^2 k_{em,qs}$. The local fields are given for $x>0$ by

$$\frac{eB_y^{loc}}{m_e\omega_{pe}c} = -i\int_{-\infty}^\infty dk_z e^{ik_z\xi}\int_{C_+} dk_x e^{ik_x x} n_{\mathbf{k}}\frac{\omega_{pe}\beta Z_b k_x\left(k_x^2 + \omega_{pe}^2/c^2\right)}{cn_p\left(k_x^2 - k_{em}^2\right)\left(k_x^2 - k_{qs}^2\right)}, \tag{14}$$

$$\frac{eE_x^{loc}}{m_e\omega_{pe}c} = -i\int_{-\infty}^\infty dk_z e^{ik_z\xi}\int_{C_+} dk_x e^{ik_x x} n_{\mathbf{k}}\frac{Z_b k_x^3\omega_{ce}^2}{cn_p\omega_{pe}\left(k_x^2 - k_{em}^2\right)\left(k_x^2 - k_{qs}^2\right)}. \tag{15}$$

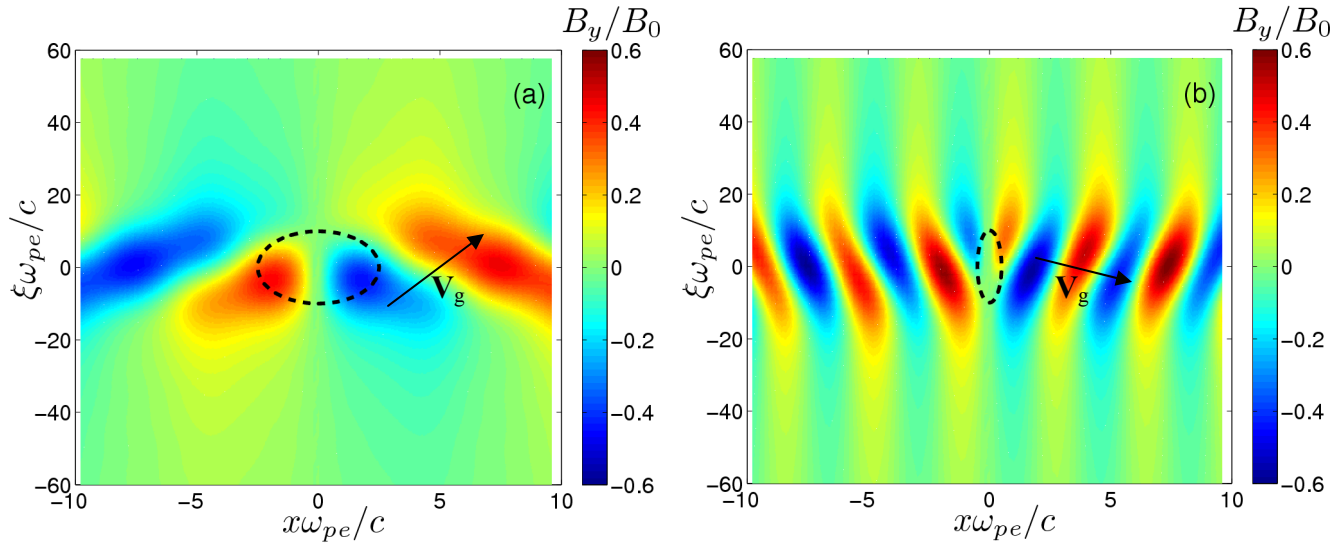

Fig. 4. Plots of the steady-state amplitude of the transverse magnetic field perturbations B_y. The beam-plasma parameters correspond to Z_b=1, l_b=10c/ω_{pe}, β_b=0.33, and n_p=2.4·10^{11} cm^{-3}. The applied magnetic field, B_{ext}=1600 G, corresponds to $\alpha=\omega_{ce}/(2\beta_b\omega_{pe})$=1.54. The frames show (a) primarily excitation of long-wavelength electromagnetic waves by a wide-aperture ion beam with r_b=2.5c/ω_{pe}; and (b) primarily excitation of short-wavelength quasi-electrostatic waves by a thin beam with r_b=0.5c/ω_{pe}. The information used in obtaining the plots is obtained from Eqs. (A1)-(A7). The normalization factor in Frames (a) and (b) is given by $B_0=4\pi n_{b0}Z_b e\beta_b r_b$. The arrows schematically illustrate the direction of the wave packet group velocity. Dashed lines correspond to the contour of constant beam density corresponding to the effective beam radius r_b.

It should be noted that for the case where the beam density profile is specified by $n_b(x,z-v_bt)=n_x(x)n_z(z-v_bt)$, the integration over the k_z-space can be carried out independently from the k_x-space integration. Therefore, the axial dependence of the local fields is determined solely by the beam density axial profile, that is $\left(E^{loc},B^{loc}\right)=n_z(z-v_bt)\Phi_{E,B}(x)$. In contrast, it is readily seen from Eqs. (10)-(13) that the wave field propagates obliquely to the beam. This implies a coupling between the transverse and longitudinal dynamics of the system, and therefore limits the validity of the slice approximation.

Features of the steady-state whistler wave excitation are shown in Fig. 4 for the following illustrative parameters: $n_b = n_{b0}\exp\left[-r^2/r_b^2-(z-v_b t)^2/l_b^2\right]$, l_b=10c/ω_{pe} (beam pulse duration $\tau_b=l_b/v_b$=30.3/ω_{pe}), v_b=0.33c, n_{b0}=0.05n_p, n_p=2.4·10^{11} cm^{-3}, and B_{ext}=1600 G. It is readily seen for a wide-aperture beam, r_b=2.5c/ω_{pe}, that the long-wavelength electromagnetic part of the whistler branch is primarily excited [Fig. 4 (a)], and the amplitude of the quasi-electrostatic wave field is exponentially small [see Eq. (12)]. In contrast, for the case of a thinner beam, r_b=0.5c/ω_{pe}, the short-wavelength quasi-electrostatic waves are primarily represented in the excited spectrum [Fig. 4(b)] due to the large excitation factor, $\left(k_{qs}^2+\omega_{pe}^2/c^2\right)$, in front of the integral in Eq. (12). Note that for the parameters in this illustrative example, $\omega_{ce}\sim\omega_{pe}$, and therefore to obtain the plots in Fig.4, we used Eqs. (A1)-(A7), which include ω_{ce}/ω_{pe} correction terms.

(c) Time evolution of the wave-field perturbations

It should be noted that the denominators in Eqs. (10)-(11) can be expressed as

$$k_{qs}^2-k_{em}^2=4\alpha\sqrt{\alpha^2-1}\,\omega_{pe}^2/c^2\,, \tag{16}$$

and it readily follows that there is strong resonant wave excitation for the case where the poles are merging, corresponding to $\alpha=\omega_{ce}/2\beta\omega_{pe}=1$ and $k_{qs}=k_{em}=\omega_{pe}/c$ [see Fig. 1(a)]. Indeed, it can be shown in the limit $\alpha=1$ that the group velocity of an excited wave packet becomes equal to the beam velocity, i.e., $V_{gx}=0$, $V_{gz}=v_b$. That is the wave packet is moving together with the beam pulse, and can therefore be amplified to very large amplitude (during a very long time interval), assuming a linear plasma response. The wave-field intensity, however, will be saturated either by nonlinear processes or due to dissipation (collisions). Note that the local fields specified by Eqs. (14)-(15) do not have singularities at $\alpha=1$.

For the case where $\alpha>1$, the wave-field amplitude reaches a finite quasi-steady-state limit with a characteristic time scale of $\tau_s\sim\min\left\{r_b/V_{gx}, l_b/\left|V_{gz}-v_b\right|\right\}$. This time interval is required for an initial transient wave packet to propagate sufficiently outside the beam pulse. For the excited wave vectors specified by Eq. (7), it can be shown that $V_{gx}/\left(V_{gz}-v_b\right)=k_x/k_z$. Therefore, for a sufficiently long beam pulse with $l_b>>k_{qs,em}^{-1}$, the wave perturbations propagates primarily in the

transverse direction, and leaves the beam in the time period $\tau_s \sim r_b/V_{gx}$. For the case where $\alpha \geq 1$ and $r_b \sim c/\omega_{pe}$, making use of Eqs. (4) and (7), we obtain $\tau_s \sim r_b/V_{gx} \sim l_b/v_b$. That is, the time scale for achieving a quasi-steady-state is of order the beam pulse duration, and is therefore much longer than the plasma period, i.e.,

$$\tau_s \sim l_b/v_b >> 1/\omega_{pe} \tag{17}$$

Note that this result is significantly different from the case B_{ext}=0, where the characteristic time to reach a quasi-steady-state is of order of the plasma period.

(d) Influence of the excited wave field on beam charge neutralization and current neutralization

It is of particular interest for neutralized beam transport applications to estimate the degrees of beam charge neutralization and current neutralization associated with the excited wave field. Here, we consider the case where $\alpha \geq 1$, and the limit where $\alpha >> 1$ and the analysis of the local-field component is addressed in Sec. V. It is convenient to introduce $E_0 = 4\pi n_{b0} Z_b e r_b$ and $B_0 = 4\pi n_{b0} Z_b e \beta_b r_b$ that represent, respectively, the characteristic transverse self-electric field and self-magnetic field generated by an ion beam propagating in vacuum. Here, n_{b0} and r_b are the characteristic values of the beam density and radius. The degrees of beam charge neutralization and current neutralization can now be effectively measured by E_x/E_0 and B_y/B_0. Considering, for simplicity, a Gaussian beam density profile with $n_{\mathbf{k}} = (r_b l_b/4\pi) n_{b0} \exp\left[-r_b^2 k_x^2/4 - l_b^2 k_z^2/4\right]$, it follows from Eqs. (10)-(13) that the degrees of beam charge neutralization and current neutralization associated with the wave field excitations is given by

$$\frac{B_y^W}{B_0} \sim \sqrt{\pi}\, \frac{\max\left\{c^2 k_{qs}^2/\omega_{pe}^2 \exp\left(-r_b^2 k_{qs}^2/4\right), \exp\left(-r_b^2 k_{em}^2/4\right)\right\}}{4\alpha\sqrt{\alpha^2-1}}, \tag{18}$$

$$\frac{E_x^W}{E_0} \sim \sqrt{\pi}\, \frac{\omega_{ce}^2}{\omega_{pe}^2} \frac{\max\left\{\left(c^2 k_{qs}^2/\omega_{pe}^2\right)\exp\left(-r_b^2 k_{qs}^2/4\right), \left(c^2 k_{em}^2/\omega_{pe}^2\right)\exp\left(-r_b^2 k_{em}^2/4\right)\right\}}{4\alpha\sqrt{\alpha^2-1}}. \tag{19}$$

It readily follows from Eqs. (18)-(19), for the case where $r_b k_{em}/2 \leq 1$ and $\alpha \geq 1$, that the beam current is not neutralized, i.e., $B_y^W/B_0 \sim 1$. The beam charge is, however, well-neutralized, i.e., $E_x^W/E_0 << 1$, provided $\omega_{ce} << \omega_{pe}$ [this is due to the factor $\omega_{ce}^2/\omega_{pe}^2$ in Eq. (19)]. For the case

where $\omega_{ce} \sim \omega_{pe}$, the degree of charge neutralization decreases, giving $E_x^W / E_0 \sim 1$, (see Appendix A), which is consistent with the analysis in Ref. [15].

III. RESONANT WAVE EXCITATION: THE ASYMPTOTIC TIME-DEPENDENT SOLUTION

In the previous section, it was demonstrated for the critical case where $\alpha = 1$, that very-large-amplitude wave-field excitations are predicted by the linear theory for a quasi-steady-state solution. This effect of large-amplitude wave-field excitations in the limit of merging poles corresponding to $\alpha = \omega_{ce} / 2\beta\omega_{pe} = 1$ and $k_{qs} = k_{em} = \omega_{pe} / c$ (so-called double pole case) has been previously reported in Refs. [22-23] for the case of an axially-continuous and thin ($r_b k_\perp << 1$) electron beam with a periodically modulated axial density profile. In those calculations, weak dissipation (due to collisions) [22], or nonlinear interaction between the beam electrons and the excited whistler waves [23] were assumed in order to estimate the saturated amplitude of the electromagnetic field perturbations. In the present analysis we obtain the asymptotic time-dependent solution for the wave amplitude in the linear approximation. Furthermore, we discuss a possible mechanism for saturation of the wave field intensity associated with the nonlinear response of the background plasma electrons, which can drive the system off resonance. Provided the beam ions are sufficiently massive, the saturation determined by this mechanism can occur before the nonlinear interaction between the beam ions and the excited whistler waves becomes important.

To describe the time-evolution of the electromagnetic field perturbation excited by the ion beam pulse, we solve here an initial-value problem, making use of Laplace transforms with respect to time. Note that the temporal Fourier transform used in Sec. II yields only the steady-state solution. In this section, we assume that the initial electromagnetic field is zero everywhere, and the beam current (source) is instantaneously turned on at t=0, i.e., $j_b = Z_b e n_b (z - v_b t, x) H(t)$, where $H(t)$ is the Heaviside step function defined by H(t)=0 for t<0, and H(t)=1 for t≥0. Similar to Eq. (3), we obtain that the space (Fourier) - time (Laplace) transform of the perturbed transverse magnetic field is given by

$$\frac{eB^y_{\omega,\mathbf{k}}}{m_e\omega_{pe}c} = -\frac{1}{2\pi}\frac{\omega_{pe}\beta_b^3 c^3 Z_b k_z^2 k_x}{n_p\left(\omega_{pe}^2 + c^2k^2\right)}\frac{n_{\mathbf{k}}}{\left[\omega^2 - \omega_{wh}^2\left(k_x,k_z\right)\right](\omega - k_z v_b)}. \tag{20}$$

The inverse Laplace time transform performed in the complex ω-plane readily gives

$$\frac{eB^y_{\mathbf{k}}}{m_e\omega_{pe}c} = -i\frac{\omega_{pe}\beta_b^3 c^3 Z_b k_z^2 k_x n_{\mathbf{k}}}{n_p\left(\omega_{pe}^2 + c^2k^2\right)}\left[\frac{\exp\left(-ik_z v_b t\right)}{k_z^2 v_b^2 - \omega_{wh}^2} + \frac{\exp\left(-i\omega_{wh}t\right)}{2\omega_{wh}\left(\omega_{wh} - k_z v_b\right)} + \frac{\exp\left(i\omega_{wh}t\right)}{2\omega_{wh}\left(\omega_{wh} + k_z v_b\right)}\right]. \tag{21}$$

Note that the first term inside the brackets in Eq. (21) corresponds to the steady-state solution [compare with Eq. (6)], in which all quantities depend on t and z exclusively through the combination $\xi = z - v_b t$. The other two terms describe the time evolution of the transient excitations. Assuming a sufficiently long beam pulse, $k_z^{-1} \sim l_b >> k_{qs,em}^{-1}$, for the double-pole case corresponding to $\alpha = \omega_{ce}/2\beta_b\omega_{pe} = 1$, Eq. (21) takes the form

$$\frac{eB^y_{\mathbf{k}}}{m_e\omega_{pe}c} = -i\frac{\omega_{pe}\beta_b^3 c Z_b k_z^2 k_x n_{\mathbf{k}}}{2\omega_{wh}k_z v_b n_p}\left[-\frac{\exp\left(-i\omega_{wh}t\right) - \exp\left(-ik_z v_b t\right)}{\left(k_x - \omega_{pe}/c\right)^2} + \frac{\exp\left(i\omega_{wh}t\right) - \exp\left(-ik_z v_b t\right)}{\left(k_x + \omega_{pe}/c\right)^2}\right]. \tag{22}$$

The right-hand side of Eq. (22) has two critical points on the real k_x-axis corresponding to $k_x = \pm\omega_{pe}/c$. However, for the case where $\alpha = 1$, the dispersion relation yields $\omega_{wh}\left(\pm\omega_{pe}/c, k_z\right) = \pm k_z v_b$. Furthermore, the x-component of the group velocity is equal to zero at the critical points, $V_{gx}\left(k_x = \pm\omega_{pe}/c, k_z\right) = 0$. Therefore, the time-dependent solution in Eq. (22) is regular at the critical points, $k_x = \pm\omega_{pe}/c$, and the inverse Fourier integration in k_x-space can be carried out along the real axis. Note that at large times, $\omega_{wh}t >> 1$, the contribution to the integral comes mainly from the regions near the points of stationary phase, where $\partial\omega_{wh}/\partial k_x \equiv V_{gx} = 0$, which coincide with the critical points $k_x = \pm\omega_{pe}/c$. The asymptotic time-dependant solution is then given by

$$\frac{eB^y_{k_z}}{m_e\omega_{pe}c} = -\frac{\omega_{pe}^2\beta_b Z_b e^{-ik_z v_b t}}{c^2 n_p} n_{\mathbf{k}}\left(\frac{\omega_{pe}}{c}, k_z\right)\sin\left(\frac{\omega_{pe}}{c}x\right)\int_{-\infty}^{\infty} d\Delta k_x \frac{\exp\left[i\,\mathrm{sgn}\left(k_z\right)\omega''_{wh}\Delta k_x^2\, t/2\right] - 1}{\Delta k_x^2}, \tag{23}$$

where $B^y_{k_z} = \int_{-\infty}^{\infty} dk_x B^y_{\mathbf{k}} e^{ik_x x}$, $\omega''_{wh} = \left|\left[\partial^2\omega_{wh}/\partial k_x^2\right]_{k_x=\omega_{pe}/c}\right| = c^3\left|k_z\right|\beta_b/\omega_{pe}^2$, and it has been assumed that $n_{\mathbf{k}}\left(\omega_{pe}/c, k_z\right) = n_{\mathbf{k}}\left(-\omega_{pe}/c, k_z\right)$. Noting that $\int_{-\infty}^{\infty} dx\left[\exp\left(\pm ix^2\right) - 1\right]/x^2 = \sqrt{2\pi}\left(\pm i - 1\right)$, we obtain

$$\frac{eB_y}{m_e\omega_{pe}c} = \sqrt{t}\,\frac{2\sqrt{\pi}\omega_{pe}v_b^{3/2}Z_b}{n_p}\sin\left(\frac{\omega_{pe}}{c}x\right)N_z(z), \tag{24}$$

where

$$N_z = \int_0^\infty dk_z\sqrt{k_z}\,n_{\mathbf{k}}\left(\frac{\omega_{pe}}{c},k_z\right)\left[\cos(k_z\xi)+\sin(k_z\xi)\right], \tag{25}$$

and a symmetric beam profile with $n_{\mathbf{k}}\left(\omega_{pe}/c,k_z\right) = n_{\mathbf{k}}\left(\omega_{pe}/c,-k_z\right)$ has also been assumed. Equations (24)-(25) describe the asymptotic evolution of the wave field for the double pole case corresponding to $\alpha = \omega_{ce}/2\beta\omega_{pe} = 1$. It is readily seen from Eq. (24) that at sufficiently large times, $\omega''_{wh}t/r_b^2 >> 1$, the amplitude of the magnetic field is given by

$$B_y \sim \sqrt{v_b t/l_b}\,Z_b e n_b \beta_b r_b, \tag{27}$$

provided the beam radius is of the order of or smaller than the electron skin depth.

As the amplitude of the resonantly-excited electromagnetic field perturbation increases, nonlinear processes can provide saturation of the energy transfer from the beam to the wave field. Here, we consider a plausible mechanism to describe saturation of the wave field intensity, in which the enhanced electromagnetic field perturbation generated by the ion beam pulse modifies properties of the whistler waves, and drives the system off resonance. Indeed, as the longitudinal component of the magnetic field perturbation B_z increases, the resonance condition becomes less accurate, $\alpha_{NL} = \omega_{ce}^{NL}/2\beta_b\omega_{pe} > 1$, where $\omega_{ce}^{NL} = e(B_0+B_z)/m_e c$. Recalling that the form of the resonance denominator is given by $1/\left(\alpha\sqrt{\alpha^2-1}\right)$, the normalized magnitude of the perturbed longitudinal magnetic field $\Delta\alpha \equiv (eB_z/m_e c)/\left(2\beta_b\omega_{pe}\right)$ can be estimated by $\Delta\alpha \sim Z_b\left(n_b/n_p\right)\left(r_b\omega_{pe}/c\right)\left[\left(1+\Delta\alpha^2\right)-1\right]^{-1/2}$ provided the beam radius is of the order of or smaller than the electron skin depth [see Eq. (B5)]. It now follows that the wave-field intensity saturates at the approximate level

$$\Delta\alpha \sim Z_b^{2/3}\left(n_b/n_p\right)^{2/3}\left(r_b\omega_{pe}/c\right)^{2/3}. \tag{28}$$

For the case of low beam density, $n_b << n_p$, this amplitude of the electromagnetic field perturbation is significantly higher compared to the case of non-resonant excitation, $\alpha > 1$, where the normalized steady-state amplitude is proportional to n_b/n_p. Finally, we emphasize that

although the mechanism considered for the wave-field intensity saturation seems plausible, further detailed analytical and numerical studies are required to validate it.

The resonant excitation of whistler waves has been observed in numerical particle-in-cell simulations performed using the two-dimensional slab (x,z) version of the LSP code[27] taking into account electromagnetic effects. As an illustrative example, we consider a Gaussian ion beam pulse, $n_b = 0.05 n_p \exp\left[-r^2/r_b^2 - (z - v_b t)^2/l_b^2\right]$, with effective beam radius r_b=0.92c/ω_{pe}, and beam pulse half-length, l_b=9.2c/ω_{pe} (beam pulse duration $\tau_b = l_b/v_b$=27.8/ω_{pe}), propagating with velocity v_b=0.33c through a background plasma with density, n_p=2.4·10^{11} cm^{-3}. In the numerical simulations, the ion beam is injected through the lower boundary of the simulation domain into an unperturbed magnetized plasma, and it propagates in the z-direction exciting electromagnetic field perturbations. Figure 5 shows the results of the numerical simulations for the time-evolution of the maximum value of the perturbed transverse magnetic field B_y. Note that for the parameters in this illustrative example, $\omega_{ce} \sim \omega_{pe}$ and β_b=0.33, and therefore a generalized analysis for arbitrary value of ω_{ce}/ω_{pe} should be carried out in order to estimate corrections to the resonance condition. The analysis shows (see Appendix A) that the resonant excitation of the wave field should occur at $\tilde{\alpha} = \omega_{ce}\left(1 - \beta_b^2\right)/\left(2\beta_b \omega_{pe}\right) = 1$ [14]. It is readily seen from Fig. 5 that as

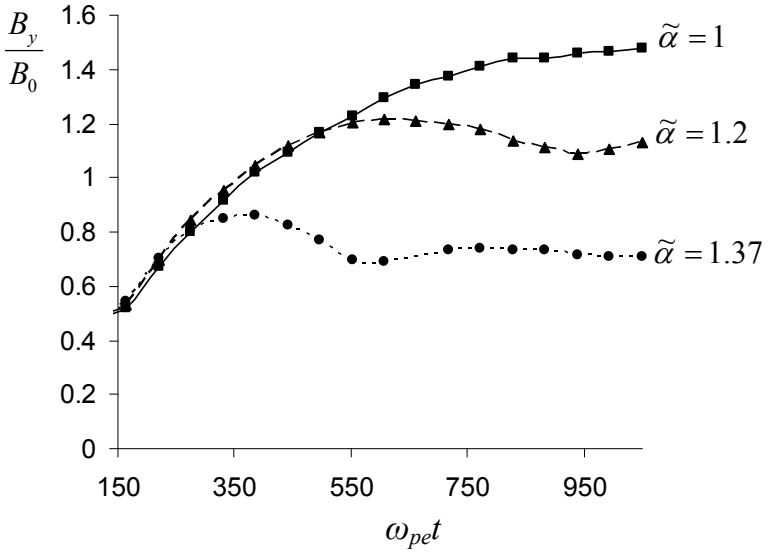

Fig. 5. Time evolution of the maximum value of the normalized perturbed transverse magnetic field plotted for different vales of the applied magnetic field. The beam-plasma parameters correspond to Z_b=1, r_b=0.92c/ω_{pe}, l_b=9.2c/ω_{pe}, β_b=0.33, and n_p=2.4·10^{11} cm^{-3}. The applied magnetic field corresponds to $\tilde{\alpha} = 1$ (solid curve), $\tilde{\alpha} = 1.2$ (dashed curve), and $\tilde{\alpha} = 1.37$ (dotted curve).

the magnitude of the applied uniform longitudinal magnetic field, B_{ext}, approaches the critical value corresponding to $\tilde{\alpha} = 1$, the saturation amplitude of the perturbed magnetic field increases, as well as the time interval required to achieve a quasi-steady-state. Note that the perturbed transverse magnetic field shown in Fig. 5 is normalized to the magnetic self-field of an unneutralized beam, $B_0 = 4\pi n_{b0} Z_b e \beta_b r_b$. It is evident, for the quasi-steady-state regime, that the beam current is unneutralized, $B_y \sim B_0$, which is consistent with the analytical analysis performed in Sec. II.

Finally, it should be noted that the effect of resonant large-amplitude wave field excitations can be utilized for diagnostics purposes in experiments where an ion beam pulse propagates through a background plasma along an applied solenoidal magnetic field [3,7-8]. Indeed, measuring the perturbed azimuthal magnetic field, for instance, in the vicinity of the chamber wall, it can be expected to obtain the following dependence on the value of the applied magnetic field. First, at low values of the applied magnetic field, $\alpha = \omega_{ce} / 2\beta_b \omega_{pe} < 1$, the wave-field component of the electromagnetic field perturbation is not excited, and the excited signal is exponentially small. As the magnetic field increases, and the threshold value of $\alpha = \omega_{ce} / 2\beta_b \omega_{pe} = 1$ is reached, a large-amplitude signal corresponding to resonant wave excitation will be detected. Finally, further increase in the magnitude of the applied magnetic field, $\alpha = \omega_{ce} / 2\beta_b \omega_{pe} > 1$, will lead to a decrease in the amplitude of the excited signal. Provided the directed beam velocity is known, this diagnostic can be used, for instance, for passive measurements of the background plasma density. Indeed, determining the threshold magnitude of the applied magnetic field, B_c, from the experimental data, the plasma density can be readily obtained from $\omega_{pe} = \omega_{ce}(B_c) / 2\beta_b$.

IV. COMPARISON OF ANALYTICAL THEORY WITH NUMERICAL SIMULATIONS

In this section we present the results of the numerical simulations performed with the particle-in-cell (PIC) code LSP and compare it with the analytical solutions described in Sec. II. Figure 6(a) shows the results obtained with the 2D slab (*x*,*z*) version of the code for the amplitude of the *y*-component of the perturbed magnetic field, when a quasi-steady-state is reached. The corresponding analytical solution [Eqs. (A1)-(A7)] is shown in Fig. 6(b). The following parameters

have been used for this illustrative example: $n_b = 0.05 n_p \exp\left[-r^2/r_b^2 - (z - v_b t)^2/l_b^2\right]$, r_b=0.92c/ω_{pe}, l_b=10r_b (beam pulse duration $\tau_b = l_b/v_b = 27.8/\omega_{pe}$), v_b=0.33c, n_p=2.4·10^{11} cm^{-3}, and B_{ext}=1600 G . It is readily seen from Figs. 6(a) and 6(b) that the results of the numerical simulations and analytical theory are found to be in very good agreement. Indeed, the characteristic amplitude of the electromagnetic field perturbation, wavelength, angle of the propagation, etc., are quite similar.

In addition, to verify the approximate analytical solution specified by Eqs. (A1)-(A7), we first solved Eq. (1) for arbitrary values of ω/ω_{ce} , ω/ω_{pe} , and ω_{pe}/ω_{ce} , and then numerically calculated the inverse *fast* Fourier transforms. Note that in the regime where a wave field is excited, the Fourier transforms of the perturbed electromagnetic fields contain singularities in real (k_x,k_z)-space. Therefore, the numerical integration of the fast Fourier transforms (FFT) performed along the real k_x- and k_z- axes would diverge. To remove the singularities from the real axis, weak collisions have been assumed for the plasma electron response. Correspondingly, the components of the dielectric tensor, $\vec{\vec{\varepsilon}}$, should be modified according to [25] $\varepsilon_{xx} = \varepsilon_{yy} = 1 - \omega_{pe}^2 (\omega + i\nu) \Big/ \left[\omega\left((\omega + i\nu)^2 - \omega_{ce}^2\right)\right]$, $\varepsilon_{zz} = 1 - \omega_{pe}^2 / \left[\omega(\omega + i\nu)\right]$, and $\varepsilon_{xy} = -\varepsilon_{yx} = i\,\omega_{pe}^2 \omega_{ce} \Big/ \left[\omega\left((\omega + i\nu)^2 - \omega_{ce}^2\right)\right]$, where ν is the effective collision frequency. In the limit of zero collision frequency, the numerical FFT calculation should yield the analytical solutions given in Eqs. (A1)-(A7). The results obtained in the numerical FFT calculation for the case of weak dissipation, ν=0.005/τ_b, demonstrate very good agreement with the analytical solution [compare Fig. 6(b) and Fig 6(c)].

It is of particular interest to compare the results obtained for the case of (x,z) slab geometry [Figs. 6(a) – 6(c)] to the case of cylindrical (r,z) geometry. The results of the numerical simulation obtained using the 2D (r,z) cylindrical version of the LSP code for the same system parameters are shown in Fig. 6(d). Results of the (r,z) LSP simulations demonstrate similar wavelength and propagation angle for the excited wave field. However, the amplitude of the perturbed electromagnetic field is smaller. Furthermore, it decays more rapidly outside the beam pulse, compared to the case of the slab beam pulse [compare Fig. 6(a) and 6(d)]. Note for an infinitely long beam that the amplitude of an excited electromagnetic field decreases as 1/r for the case of cylindrical geometry, and does not decrease for the case of 2D slab geometry. This can provide a

plausible explanation of the difference in the wave-field amplitude observed in cylindrical and slab geometries.

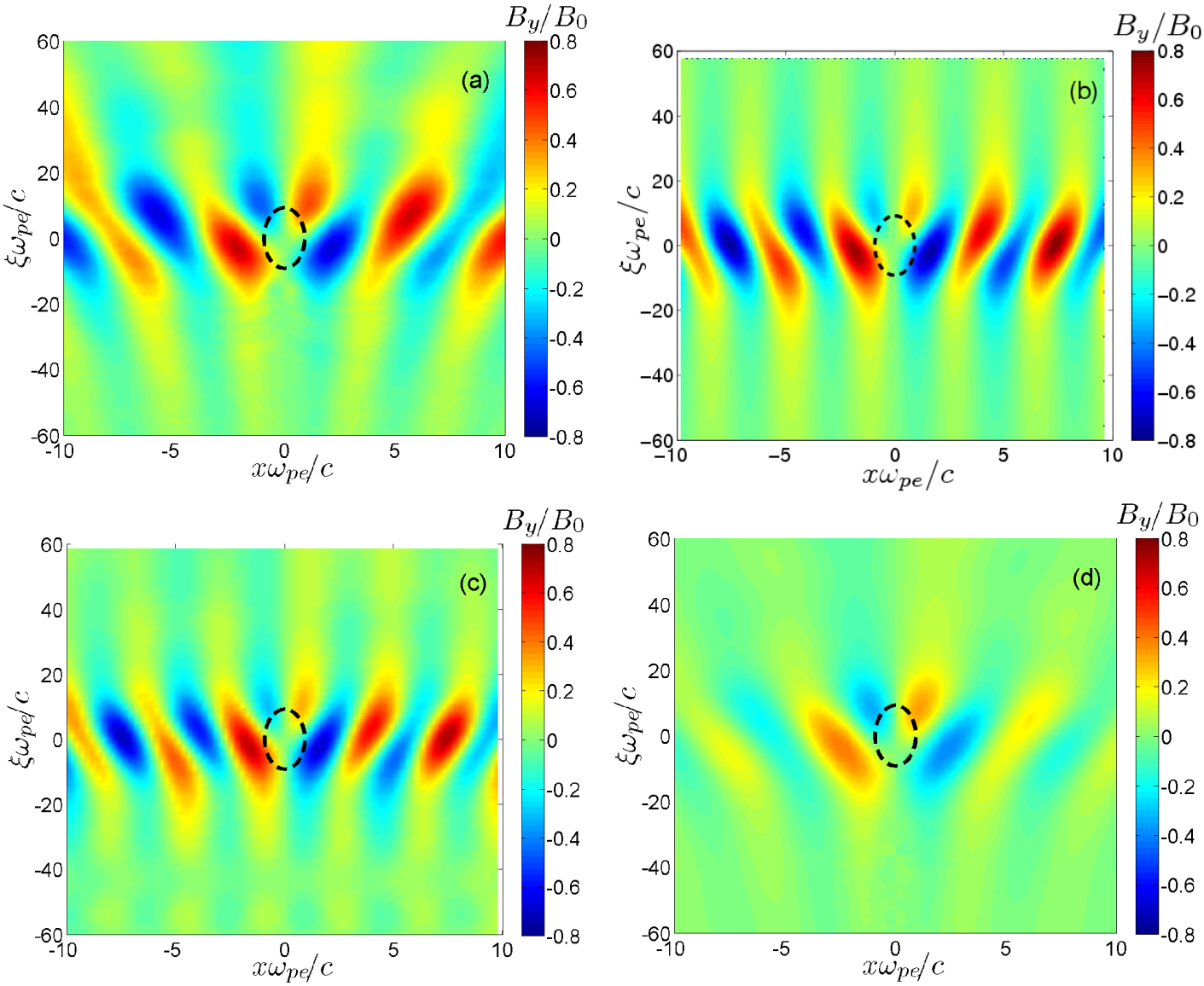

Fig. 6. Plots of the steady-state amplitude of the transverse magnetic field perturbation B_y. The beam-plasma parameters correspond to Z_b=1, r_b=0.92c/ω_{pe}, l_b=10r_b, β_b=0.33, and n_p=2.4·10^{11} cm^{-3}. The applied magnetic field, B_{ext}=1600 G, corresponds to $\alpha=\omega_{ce}/(2\beta_b\omega_{pe})$=1.54. The Frames correspond to: (a) results of numerical simulations obtained using the (x,z) slab version of the LSP code; (b) the analytical solution given by Eqs. (A1)-(A7); (c) numerical calculation of fast Fourier transforms, assuming weak collisions $\nu=0.005/\tau_b$; and (d) the results of numerical simulations obtained using the (r,z) cylindrical version of the LSP code. The dashed lines correspond to contours of constant beam density corresponding to the effective beam radius r_b.

V. SELF-FOCUSING OF AN INTENSE ION BEAM PULSE

In this section, making use of Eqs. (10)-(15), we calculate the transverse component of the Lorentz force, $F_x = Z_b eE_x - Z_b e\beta_b B_y$, acting on the beam particles. In Sec. II it has been shown that the excited wave field perturbations propagate oblique to the beam with characteristic longitudinal wave number $k_z \sim l_b^{-1}$. Therefore, the contribution of the wave-field component to the total Lorentz force can have opposite signs for the beam head and the beam tail. That is, it produces a focusing effect in the beam head and a defocusing effect in the beam tail, or *vise verse*. In contrast, the longitudinal profile of the local-field amplitude is the same as the longitudinal beam density profile (see Sec. II). Therefore, the local fields provide a focusing (or defocusing) effect over the entire length of the ion beam pulse. It is therefore important, in practical applications involving control over the beam aperture, to identify the parameter regimes where the local component of the electromagnetic field perturbation has the dominant influence on the beam transverse dynamics.

(a) Regimes of dominant influence of local fields on the beam transverse dynamics

It has been demonstrated in Sec. II for the critical case where $\alpha = 1$, that a large-amplitude wave field is exited. Here, we consider the case where $\alpha >> 1$ ($\omega_{ce} >> 2\beta_b \omega_{pe}$). Furthermore, we assume $r_b >> k_{qs}^{-1}$, or equivalently, $r_b >> c/(2\alpha\omega_{pe})$ in the limit where $\alpha >> 1$. This implies an exponentially small level of the short-wavelength, quasi-electrostatic wave excitations for the case of a smooth radial beam density profile. Making use of Eqs. (10)-(13), it is straightforward to show for the case where $r_b >> k_{qs}^{-1}$, that the contribution of the wave-field component of the electromagnetic field perturbation to the transverse Lorentz force is given approximately by

$$F_x^W = Z_b e\left(E_x^W - \beta_b B_y^W\right) \approx 2\pi Z_b^2 \frac{m_e V_b^2}{R} \frac{1-\left(4\alpha^2-1\right)k_{em}^2 c^2/\omega_{pe}^2}{4\alpha\sqrt{\alpha^2-1}}, \tag{29}$$

where

$$\frac{1}{R} = \frac{\omega_{pe}^2}{c^2}\frac{1}{n_p}\int_0^\infty dk_z n_{\mathbf{k}}\left(k_{em}, k_z\right)\cos\left[k_z\xi + k_{em}x\right]. \tag{30}$$

Recall, for $\alpha >> 1$, that the characteristic wave vector for the excited long-wavelength electromagnetic wave field is given by $k_{em} = \omega_{pe} / 2\alpha c$, and therefore the wave field contribution to the Lorentz force vanishes for $\alpha >> 1$. To obtain the local field contribution, it is convenient to represent the local fields specified by Eqs. (14)-(15) in the following form

$$e\beta_b B_y^{loc} = -iZ_b m_e v_b^2 \int d\mathbf{k} \frac{k_x \left(k_x^2 + \omega_{pe}^2 / c^2\right) n_{\mathbf{k}} e^{ik_x x + ik_z \xi}}{4\alpha\sqrt{\alpha^2 - 1} n_p} \left[\frac{1}{k_x^2 - k_{qs}^2} - \frac{1}{k_x^2 - k_{em}^2}\right], \tag{31}$$

$$eE_x^{loc} = -iZ_b m_e v_b^2 \int d\mathbf{k} \frac{\alpha k_x^3 n_{\mathbf{k}} e^{ik_x x + ik_z \xi}}{\sqrt{\alpha^2 - 1} n_p} \left[\frac{1}{k_x^2 - k_{qs}^2} - \frac{1}{k_x^2 - k_{em}^2}\right]. \tag{32}$$

For the case where

$$\alpha >> 1 \text{ and } r_b >> k_{qs}^{-1} = \frac{c}{2\alpha\omega_{pe}} \tag{33}$$

we can neglect by the first terms inside the brackets in Eqs. (31) and (32), and after some straightforward algebra we obtain that the local field contribution, which constitutes most of the transverse Lorentz force, is given by

$$F_x \approx Z_b eE_x^{loc} - Z_b e\beta_b B_y^{loc} = Z_b^2 m_e v_b^2 \frac{1}{n_p} \frac{dn_b}{dx}. \tag{34}$$

The analysis in Appendix A, performed for an arbitrary ratio of $\omega_{ce} / \omega_{pe}$, shows that for the case of a nonrelativistic ion beam the Lorentz force is still given by Eq. (34), provided

$$\alpha >> 1 \text{ and } r_b >> \tilde{k}_{qs}^{-1} = \left(1 + \omega_{ce}^2 / \omega_{pe}^2\right)^{1/2} \frac{c}{2\alpha\omega_{pe}}. \tag{35}$$

Note that the transverse component of the Lorentz force [Eq. (34)] is proportional to the gradient of the beam density. Therefore, for the case of a bell-shaped beam density profile, self-focusing of the beam occurs. Furthermore, it is interesting to note that an annular beam will not pinch to the axis provided the beam dynamics is governed by the force in Eq. (34). However, the outer beam radius will decrease and the inner beam radius will increase, resulting in a decrease in the thickness of the annulus and an increase in the beam density.

Although the total influence of the magnetic and electric field components, B_y^W and E_x^W, of the wave field perturbation results in a destructive interference in estimating the transverse Lorentz force [see Eq. (29)], it is of particular interest to estimate the separate contribution of the wave

field component to the Lorentz force, and compare it to the contribution of the local field component. For illustrative purposes, we consider here a Gaussian beam density profile with $n_{\mathbf{k}} = (r_b l_b/4\pi) n_{b0} \exp\left[-r_b^2 k_x^2/4 - l_b^2 k_z^2/4\right]$. Making use of Eqs. (10)–(13), it is straightforward to show that the contribution of the wave field component can be estimated by

$$eE_y^W \sim e\beta_b B_y^W \sim Z_b m_e V_b^2 \frac{\omega_{pe}^2 r_b}{\alpha^2 c^2} \frac{n_{b0}}{n_p} \exp\left(-\frac{r_b^2 k_{em}^2}{4}\right), \tag{36}$$

provided the conditions in Eq. (33) are satisfied. Similar expressions can be obtained for the local fields using Eqs. (31)-(32), i.e.,

$$eE_x^{loc} \sim Z_b m_e V_b^2 \frac{n_{b0}}{r_b n_p} \frac{1}{\max\left(1, k_{em}^2 r_b^2\right)}, \tag{37}$$

$$e\beta_b B_y^{loc} \sim Z_b m_e V_b^2 \frac{n_{b0}}{\alpha^2 r_b n_p} \frac{\max\left(1, \omega_{pe}^2 r_b^2/c^2\right)}{\max\left(1, k_{em}^2 r_b^2\right)}, \tag{38}$$

It readily follows from Eqs. (36)-(38), for the case where the beam radius is small compared to the wavelength of the long-wavelength electromagnetic waves, $r_b k_{em} << 1$, that the *local electric field* has the dominant contribution to the transverse component of the Lorentz force. As the beam radius increases and becomes of order the electromagnetic wave-field wavelength, $r_b k_{em} \sim 1$, the separate contributions from all components of the perturbed electromagnetic field become of the same order, i.e., $E_x^{loc} \sim E_x^W \sim \beta_b B_x^{loc} \sim \beta_b B_x^W$. With a further increase in the beam radius, $r_b k_{em} >> 1$, the *local magnetic field* contribution becomes dominant, and both the quasi-electrostatic and long-wavelength electromagnetic wave-field components are exited to exponentially small levels for the case of a smooth beam density profile.

The time evolution of the electromagnetic field perturbation for the case where $\alpha >> 1$ and $k_{qs}^{-1} << r_b << k_{em}^{-1}$, which corresponds to a dominant influence of the local self-electric field, has been studied using the LSP simulation code. Figure 7 shows a plot of the perturbed transverse self-electric field at the simulation time t_s=54 ns. The beam-plasma parameters considered for this illustrative example correspond to $n_b = 0.13 n_p \exp\left[-r^2/r_b^2 - (z - v_b t)^2/l_b^2\right]$, n_p=10^{10}cm^{-3}, Z_b=1, r_b=$0.55c/\omega_{pe}$, τ_b=$75/\omega_{pe}$, β_b=0.05, B_{ext}=300 G, and α=$\omega_{ce}/2\beta_b\omega_{pe}$=9.35. The wave structure in front of the beam pulse corresponds to a transient wave-field perturbations associated with the initial beam penetration into the plasma through the boundary at $z = 0$. Note that these transient

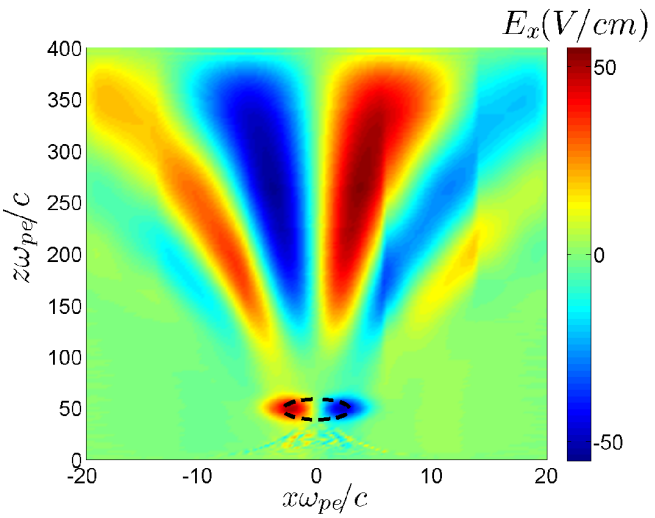

Fig. 7. Plot of the perturbed transverse self-electric field corresponding to t_s=54 ns. The system parameters correspond to Z_b=1, r_b=0.55c/ω_{pe}, τ_b=75/ω_{pe}, β_b=0.05, B_{ext}=300 G, and $\alpha=\omega_{ce}/2\beta_b\omega_{pe}$=9.35. The results are obtained using the 2D (x,z) version of the LSP code. The dashed curve corresponds to the contour of constant beam density corresponding to the effective beam radius r_b.

perturbations do not interact with the ion beam pulse effectively, because they do not satisfy the Cherenkov criteria in Eq. (7). Therefore, the energy content in the corresponding wave field is attributed only to the initial beam penetration into the plasma, and is not related to the beam energy later in time. As the transient wave-field perturbations leave the beam on the characteristic time scale τ_s~min$\{r_b/V_{gx}, l_b/|V_{gz}-v_b|\}$ (see Sec. II), the local component of the self-electric field exhibits the dominant influence on the ion beam transverse dynamics, as evident from Fig. 7. The intensity of the excited wave field satisfying the condition in Eq. (7) is negligible, which is consistent with the analytical calculations performed in this section.

(b) Enhanced ion beam self-focusing

In Sec. V (a), it was demonstrated for the case where $\alpha = \omega_{ce}/2\beta_b\omega_{pe} >> 1$ and $r_b >> c/(2\alpha\omega_{pe})$, that the local fields have the dominant influence on the transverse dynamics of the ion beam particles. In this regime, focusing is provided over the entire length of the beam pulse and the corresponding self-focusing force acting on the beam ions is specified by Eq. (34). It is of particular interest to compare this self-focusing force to the self-pinching force acting on the ion

beam particles for the case where the ion beam pulse propagates through an unmagnetized plasma, i.e., B_{ext}=0. Indeed, even for this simple case the beam charge is typically better neutralized than the beam current, and the self-pinching force is produced by the net self-magnetic field[28]. This self-pinching can be utilized for a variety of applications, including self-pinched ion beam transport[29], and heavy ion beam focusing[30]. Note that for the case where B_{ext}=0, the beam current is almost unneutralized in the limit where the beam radius is small compared to the electron skin depth, $r_b << c/\omega_{pe}$. Therefore, the self-pinching effect is a maximum in this regime.

For the case where $r_b << c/\omega_{pe}$, the ratio of the collective self-focusing force in the presence of an applied magnetic field [Eq. (34)] to the self-pinching force, F_0, in the limit B_{ext}=0 case, can be estimated as $F_x/F_0 \sim \left(c/r_b\omega_{pe}\right)^2 >> 1$ [31]. That is, the self-focusing of an ion beam pulse propagating through a neutralizing plasma can be significantly enhanced by the application of a solenoidal magnetic field satisfying $\alpha = \omega_{ce}/2\beta_b\omega_{pe} >> 1$. Here, we emphasize again that the threshold value $\alpha_{cr} = 1$ typically corresponds to a weak magnetic field (see Introduction). The condition $r_b << c/\omega_{pe}$ can be rewritten in terms of the beam current I_b as $I_b << 4.25\beta_b\left(n_b/n_p\right)\text{kA}$. Also, note that for a typical ion beam injector aperture of the order of 1 cm, the beam radius (~ 1 cm) is small compared to the electron skin depth provided the beam and plasma density are in the range of $n_b < n_p < 2.8\cdot 10^{11}/\left(r_b[cm]\right)^2\ cm^{-3}$, which are typical parameters for several beam transport applications [3,7-8]. Therefore, this self-focusing enhancement can be of considerable practical importance.

As a practical example, here we consider parameters characteristic of the present Neutralized Drift Compression Experiment (NDCX-I) [7] and its future upgrade NDCX-II [8], which are designed to study the energy deposition from the intense ion beam onto a target. The experiments involve neutralized compression of an intense ion beam pulse with radius r_b~1 cm as it propagates through a long drift section with length L_d~200 cm filled with a background plasma with density n_p~10^{11} cm^{-3}. As it exits the drift section, the beam passes through a strong magnetic lens with magnetic field B_s=8 T, and length L_s~10cm, which provides additional transverse focusing. For the currently operating NDCX-I experiment, typical beam parameters correspond to $\beta_b^I = 0.004$, $m_i^I = 39$ a.u., $Z_b^I = 1$. The proposed NDCX-II experiment is aimed at operating at higher beam energies: $\beta_b^{II} = 0.032$, $m_i^{II} = 7$ a.u., $Z_b^{II} = 1$. The corresponding values of the critical

magnetic field are given by $B_c^I = 130$ G and $B_c^{II} = 16$ G, for NDCX-I and NDCX-II parameters, respectively. The fringe magnetic field of the strong magnetic lens can penetrate deeply into the drift section at a magnitude much larger than $B_c^{I,II}$, thus providing conditions for enhanced self-focusing for both NDCX-I and NDCX-II. Moreover, the integrated effect of the beam self-focusing inside the drift section filled with the background plasma can become comparable to the focusing effect of the strong magnetic lens. Introducing the dimensionless parameters $\delta = F_{sf} L_d / F_s L_s$, where $F_s \sim m_b \omega_{cb}^2 r_b / 4$ is the magnetic focusing force acting on the beam ions inside the lens, and $F_{sf} \sim m_e V_b^2 / r_b$ is the self-focusing force ($n_b \sim n_e$ is assumed), we readily obtain $\delta^I = 0.04$ and $\delta^{II} = 0.5$ for the parameters characteristic of NDCX-I and NDCX-II respectively. Here, m_b and ω_{cb} are the ion beam mass and cyclotron frequency, respectively. Therefore, the plasma-induced collective focusing effect in a several hundred gauss magnetic field can become comparable to the focusing effect of a strong 8 Tesla final focus solenoid for the design parameters characteristic of NDCX-II.

It should be noted that Eq. (34), along with the conditions in Eq. (35) have been obtained previously in Ref. [31]. The analysis in Ref. [31] was performed for the case of cylindrical geometry and assumed the slice approximation, which describes very well the local fields, and is of limited validity for the case where a strongly pronounced wave field perturbation is excited [see. Sec. II]. Note that in this work we have demonstrated the dominant influence of the local fields for the case where $\alpha >> 1$ and $r_b k_{qs}^{-1} >> 1$, thus validating the assumptions used in the analysis in Ref. [31].

In addition, in the present work the enhancement of the self-focusing force in the presence of a weak applied magnetic field has been observed in electromagnetic particle-in-cell simulations performed using the 2D (x,z) slice version of the LSP code. As an illustrative example, we consider a Gaussian ion beam pulse, $n_b = 0.13 n_p \exp\left[-r^2/r_b^2 - (z - v_b t)^2 / l_b^2\right]$, with effective beam radius, $r_b = 0.55 c/\omega_{pe}$, and beam pulse half-length, $l_b = 1.875 c/\omega_{pe}$ (beam pulse duration $\tau_b = 75/\omega_{pe}$), propagating with velocity $v_b = 0.05c$ through a background plasma with density $n_p = 10^{10}$ cm^{-3}. The results of the numerical simulations shown in Fig. 8 demonstrate the significant (~10 times) enhancement of the transverse component of the Lorentz force due to an applied magnetic field of

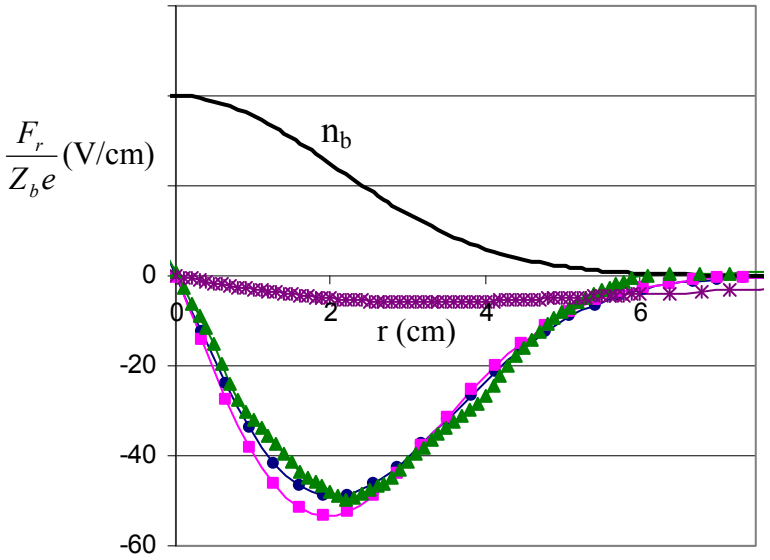

Fig. 8. Radial dependence of the normalized focusing force at the beam center. The results of the numerical simulations correspond to B_{ext}=300 G and $\alpha=\omega_{ce}/2\beta_b\omega_{pe}$=9.35 (green curve), and ω_{ce}=0 (purple curve). The analytical results in Eq. (33), are shown by the blue curve, the pink curve demonstrates the analytical predictions obtained by performing integration in Eqs. (A1)-(A7). The beam-plasma parameters correspond to Z_b=1, $r_b=0.55c/\omega_{pe}$, $\tau_b=75/\omega_{pe}$, β_b=0.05, and $n_p=10^{10}$ cm^{-3}. The black curve corresponds to the radial beam density profile.

B_{ext}=300 G. Figure 8 shows the *total* transverse focusing force (i.e., the sum of the magnetic and electric component of the Lorentz force) acting on the beam ions in the presence of an applied magnetic field (green, blue, and pink curves), and for the case where an external magnetic field is not applied (purple curve). The units of the electric field, *V/cm*, are chosen for practical representation of its numerical value. Note that the results of the numerical simulations are found to be in very good agreement with the approximate analytical solution given by Eq. (34) (blue curve), and with the more accurate analytical solutions given by Eqs. (A1)-(A7) (pink curve).

(c) Properties of a local plasma response

As demonstrated above, the local component of the self-electric field provides the dominant contribution to the transverse Lorentz force for the case where $\alpha = \omega_{ce}/2\beta_b\omega_{pe} >> 1$ and

$k_{qs}^{-1} << r_b << k_{em}^{-1}$ (or equivalently, $c/2\alpha\omega_{pe} << r_b << 2\alpha c/\omega_{pe}$). Form Eq. (34) it now readily follows that

$$Z_b e E_x \approx Z_b^2 m_e v_b^2 \frac{1}{n_p}\frac{dn_b}{dx}, \tag{39}$$

and therefore, for the case of a bell-shaped beam density profile, the transverse electric self-field produces a focusing effect on the ion beam pulse. This implies that a positive charge of the ion beam pulse becomes *over-compensated* by the background plasma electrons[31]. In the same parameter regime, the *z*-component of the magnetic field perturbation is specified by (see Appendix B)

$$\frac{eB_z^{loc}}{m_e\omega_{pe}c} \approx -\frac{Z_b\beta_b^2\omega_{pe}}{\omega_{ce}n_p} n_b(x,z), \tag{40}$$

indicating the diamagnetic plasma response.

It is interesting to note that a defocusing self-electric field and a paramagnetic plasma response were found for the case where $\alpha < 1$ [14-15]. This means that the qualitatively different local plasma responses for the cases where $\alpha < 1$ and $\alpha > 1$ are separated by the critical case where $\alpha = 1$, corresponding to resonant excitation of a large-amplitude wave-field perturbation.

The analytical calculation demonstrating the dramatic change of the local plasma response with an increase of an applied magnetic field has also been verified by the results of 2D (*x*,*z*) LSP simulations (Fig. 9). The parameters chosen for the illustrative example in Fig. 9 correspond to $n_b = 0.13 n_p \exp\left[-r^2/r_b^2 - (z - v_b t)^2/l_b^2\right]$, r_b=0.55c/ω_{pe}, l_b=1.875c/ω_{pe}, v_b=0.05c, and n_p=10^{10} cm^{-3}. One can readily see that the paramagnetic plasma response [Fig, 9(b)], and the defocusing effect of the transverse self-electric field [Fig. 9(a)] for the case where $\alpha = 0.78$, change to a diamagnetic plasma response [Fig. 9(d)] and a focusing effect of the self-electric field [Fig. 9(c)] for $\alpha = 9.35$. Note that the longitudinal oscillations in Fig. 9(a) are an artifact of the numerical code, and a smooth longitudinal dependence can be obtained by increasing the space-time resolution along with the number of macro-particles. Figures 9(e) and 9(f) show the approximate analytical solutions for the transverse component of the electric field [Eq. (26)], and the longitudinal component of the magnetic field [Eq. (27)], respectively. Finally, note that the magnitude of the transverse electric field perturbation is significantly increased by an increase in the applied

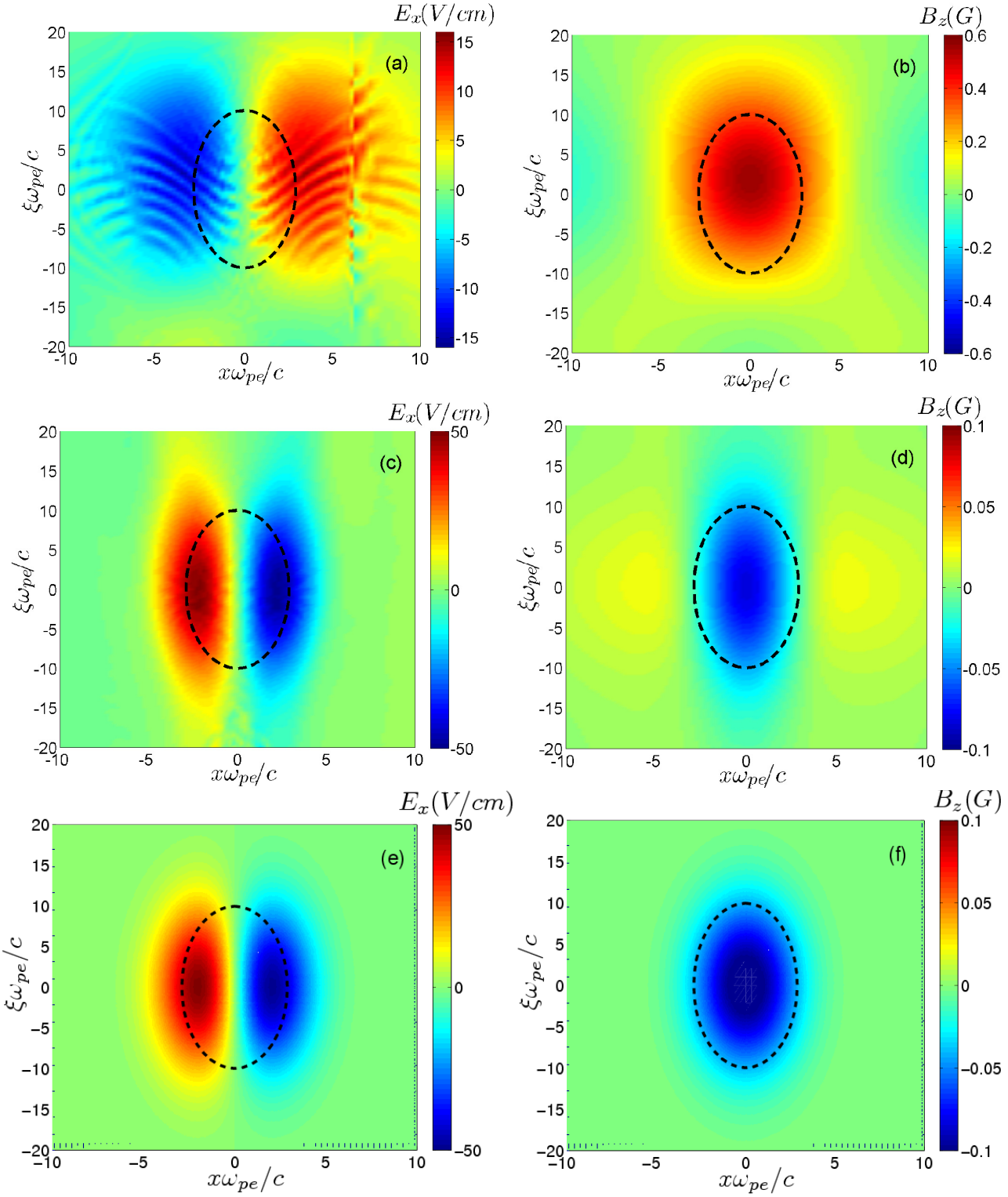

Fig. 9. Plots of the transverse self-electric field (left) and longitudinal self-magnetic (right) field of an ion beam pulse with Z_b=1, r_b=0.55c/ω_{pe}, l_b=1.875c/ω_{pe}, and v_b=0.05c propagating through a background plasma with n_p=10^{10} cm^{-3} along a solenoidal magnetic field. Frames (a) and (b) correspond to the results of 2D (x,z) LSP simulations for B_{ext}=25 G. Frames (c) and (d) correspond to the results of 2D (x,z) LSP simulations for B_{ext}=300 G. Frames (e) and (f) correspond to the approximate analytical solutions given by Eq. (38) and Eq. (39), respectively. Note the significantly different local plasma responses between the cases where α=0.78 [Frames (a) and (b)] and α=9.35 [Frames (c) and (d)]. Dashed lines correspond to contours of constant beam density corresponding to the effective beam radius r_b.

magnetic field [compare Figs. 9(a) and 9(c)]. This strong transverse electric field provides the enhanced ion beam focusing, as discussed above.

VI. CONCLUSIONS

In the present paper, the electromagnetic field perturbation excited by a long ion beam pulse propagating through a neutralizing background plasma along a solenoidal magnetic field was studied analytically, and by means of numerical simulations using the electromagnetic particle-in-cell code LSP. It was demonstrated that the total electromagnetic field perturbation excited by an ion beam pulse with a smooth radial density profile can be conveniently represented as the sum of a local-field component, rapidly decaying to zero outside the beam pulse, and a wave-field component that can extend far outside the beam. The wave field is represented by a long-wavelength electromagnetic component with $|k_x|=k_{em}<\omega_{pe}/c$, and a short-wavelength quasi-electrostatic component with $|k_x|=k_{qs}>\omega_{pe}/c$. Note that the longitudinal component of the electromagnetic wave group velocity is greater than the beam velocity. Therefore, the long-wavelength electromagnetic perturbations excited by the tail of the beam pulse can propagate along the beam and influence the dynamics of the beam head. The system reaches a quasi-steady-state when the wave packet of the initial transient excitation propagates sufficiently far outside the beam. It was found, for a sufficiently long ion beam pulse, that the time-scale for achieving a quasi-steady-state can be of order the beam pulse duration, and is therefore much longer than the inverse plasma frequency. This result is significantly different from the case $B_{ext}=0$, where the characteristic time to reach a steady-state is of the order of the plasma period.

It was also shown that the wave-field excitations propagate obliquely to the beam with a characteristic wavelength of $k_z\sim 1/l_b$. Therefore, their contributions to the transverse component of the Lorentz force can have opposite signs for the beam head and the beam tail. In contrast, the longitudinal profile of the local-field amplitude is the same as the longitudinal beam density profile. Therefore, the transverse local fields have the same sign over the entire length of the ion beam pulse. It is therefore important, in practical applications involving control over the beam aperture, to identify the parameter regimes where the local component of the electromagnetic field perturbation has the dominant influence on the beam transverse dynamics.

In this paper, it was also demonstrated, in the regime where $\omega_{ce} >> 2\beta_b\omega_{pe}$ and $r_b k_{qs} >> 1$, that the local-field component primarily determines the transverse dynamics of the beam particles;

and the wave fields produce a negligible transverse force. Moreover, a positive charge of the ion beam pulse becomes over-compensated by the plasma electrons, and the associated strong transverse-focusing self-electric field has the dominant influence on the beam ions, compared with the magnetic field, provided $k_{qs}^{-1} << r_b << k_{em}^{-1}$. It was also shown, for the case where the beam radius is small compared to the electron skin depth, that the self-focusing force is significantly enhanced compared to the self-focusing force acting of the beam particles in the absence of an applied magnetic field. In addition, the local diamagnetic plasma response is observed in the numerical simulations, and is also predicted analytically for $\omega_{ce} >> 2\beta_b\omega_{pe}$. Note that these results differ significantly from the case $\omega_{ce} < 2\beta_b\omega_{pe}$, where the transverse electric field is defocusing, and the plasma response is paramagnetic. The qualitatively different local plasma responses are separated by the critical field case where $\omega_{ce}^{cr} = 2\beta_b\omega_{pe}$, corresponding to the resonant excitation of large-amplitude wave-field perturbations. In the present analysis, the asymptotic time-dependent solution was obtained for this critical case, and the saturated intensity of the wave-field perturbations, determined from the nonlinear response of the background plasma electrons, was estimated. In addition, a plausible application of the resonant wave excitation effect for diagnostic purposes was discussed.

Finally, we emphasize that the effects of an applied solenoidal magnetic field on neutralized ion beam transport described in this paper for the case of $\omega_{ce} > 2\beta_b\omega_{pe}$ can be of particular importance for the presently operating Neutralized Drift Compression Experiment NDCX-I [7] and its future upgrade NDCX-II [8]. The design of the NDCX facilities first involves the neutralized drift compression of the ion beam pulse, and then additional transverse focusing on the target plane by a strong (several Tesla) final-focus solenoid. The threshold magnetic field in the inequality $\omega_{ce} > 2\beta_b\omega_{pe}$ corresponds to a relatively weak magnetic field of the order of 10 G (for NDCX-I) and 100 G (for NDCX-II). Therefore, the magnetic fringe fields of the final-focus solenoid above this value can penetrate deep into the drift section. In particular, these fringe fields provide conditions for enhanced beam self-focusing, which can have a significant influence on the transverse beam dynamics for the parameters characteristic of NDCX-II.

APPENDIX A: ELECTROMAGNETIC FIELD PERTURBATIONS FOR THE CASE OF ARBITRARY RATIO OF ω_{ce}/ω_{pe}

Equations (10)-(15) can be generalized to the case of an arbitrary ratio of ω_{ce}/ω_{pe}. Assuming $\omega \sim v_b/l_b << \omega_{pe}, \omega_{ce}$ and $l_b >> r_b, \tilde{k}_{em,qs}^{-1}$, after some straightforward algebra one can show that the electromagnetic field perturbations for $0 < x << l_b^2 \tilde{k}_{em,qs}$ are given by

$$\frac{eB_y^W}{m_e \omega_{pe} c} = \frac{2\pi \omega_{pe} \beta_b Z_b}{c n_p \left(\tilde{k}_{qs}^2 - \tilde{k}_{em}^2 \right)} \left(b_{em} + b_{qs} \right), \tag{A1}$$

$$\frac{eE_x^W}{m_e \omega_{pe} c} = \frac{2\pi Z_b \omega_{ce}^2}{c n_p \omega_{pe} \left(\tilde{k}_{qs}^2 - \tilde{k}_{em}^2 \right)} \left(e_{em} + e_{qs} \right), \tag{A2}$$

$$b_{qs,em} = \pm \left(\tilde{k}_{qs,em}^2 + \frac{\omega_{pe}^2}{c^2 \left(1 + \omega_{ce}^2/\omega_{pe}^2 \right)} \right) \int_0^\infty dk_z n_{\mathbf{k}} \left(\tilde{k}_{qs,em}, k_z \right) \cos\left(k_z \xi \mp \tilde{k}_{qs,em} x \right), \tag{A3}$$

$$e_{qs,em} = \pm \left[\tilde{k}_{qs,em}^2 / \left(1 + \omega_{ce}^2/\omega_{pe}^2 \right) \right] \int_0^\infty dk_z n_{\mathbf{k}} \left(\tilde{k}_{qs,em}, k_z \right) \cos\left(k_z \xi \mp \tilde{k}_{qs,em} x \right), \tag{A4}$$

$$\frac{eB_y^{loc}}{m_e \omega_{pe} c} = -i \int_{-\infty}^{\infty} dk_z e^{ik_z \xi} \int_{C_+} dk_x e^{ik_x x} n_{\mathbf{k}} \frac{\omega_{pe} \beta_b Z_b k_x}{c n_p \left(k_x^2 - \tilde{k}_{em}^2 \right) \left(k_x^2 - \tilde{k}_{qs}^2 \right)} \left(k_x^2 + \frac{\omega_{pe}^2/c^2}{1 + \omega_{ce}^2/\omega_{pe}^2} \right), \tag{A5}$$

$$\frac{eE_x^{loc}}{m_e \omega_{pe} c} = -i \int_{-\infty}^{\infty} dk_z e^{ik_z \xi} \int_{C_+} dk_x e^{ik_x x} n_{\mathbf{k}} \frac{Z_b k_x^3 \omega_{ce}^2 / \left(1 + \omega_{ce}^2/\omega_{pe}^2 \right)}{c n_p \omega_{pe} \left(k_x^2 - \tilde{k}_{em}^2 \right) \left(k_x^2 - \tilde{k}_{qs}^2 \right)}. \tag{A6}$$

Here, $\tilde{k}_{em,qs}$ are the solutions to the generalized dispersion relation

$$c^4 k_x^4 \left(1 + \frac{\omega_{pe}^2}{\omega_{ce}^2} \right) + \left[\frac{2\omega_{pe}^4}{\omega_{ce}^2} - \frac{\left(1 - \beta_b^2 \right) \omega_{pe}^2}{\beta_b^2} \right] c^2 k_x^2 + \frac{\omega_{pe}^6}{\omega_{ce}^2} = 0. \tag{A7}$$

Equations (A1)-(A7) describe the electromagnetic field perturbation excited by an ion beam pulse for an arbitrary ratio of ω_{ce}/ω_{pe}, and furthermore for an arbitrary beam velocity, including the case of a relativistic ion beam. The dynamics of the background plasma electrons, however, are assumed to be nonrelativistic, which requires that the beam density be much smaller the plasma density ($n_b << n_p$).

The onset of wave generation, corresponding to the existence of real solutions to Eq. (A7), is now determined by the condition $\tilde{\alpha} = \omega_{ce}\left(1-\beta_b^2\right)/2\beta_b\omega_{pe} > 1$. In the limit where $\tilde{\alpha} >> 1$ and $\beta_b << 1$, the solutions to Eq. (A7) can be approximated by $\tilde{k}_{qs} = 2\alpha\omega_{pe}\Big/\left[c\left(1+\omega_{ce}^2/\omega_{pe}^2\right)^{1/2}\right]$ and $\tilde{k}_{em} = \omega_{pe}/(2\alpha c)$, where $\alpha = \omega_{ce}/2\beta_b\omega_{pe}$. Making use of Eqs. (A1)-(A6), we can then reproduce the main results obtained earlier in the present paper. Repeating the analysis performed in Sec. III, after some straightforward algebra, we find that the asymptotic time-dependent solution for the critical case corresponding to $\tilde{\alpha} = 1$ is given by

$$\frac{eB^y}{m_e\omega_{pe}c} = 4\sqrt{\pi}\sqrt{t}\,\frac{\beta_b^2\tilde{k}_c\omega_{pe}Z_b\sin\left(\tilde{k}_c x\right)N_z(z)}{n_p\left(\tilde{k}_c^2+\omega_{pe}^2/c^2\right)\sqrt{\left|\partial^2\tilde{V}_z^{ph}/\partial k_x^2\right|_{k_x=\tilde{k}_c}}}, \tag{A8}$$

$$N_z = \int_0^\infty dk_z\sqrt{k_z}\,n_{\mathbf{k}}\left(\tilde{k}_c,k_z\right)\left[\cos\left(k_z\xi\right)+\sin\left(k_z\xi\right)\right], \tag{A9}$$

where the critical value of the wave vector, $\tilde{k}_c$, corresponding to the solution of Eq. (A7) for $\tilde{\alpha} = 1$, is given by

$$\tilde{k}_c = \left(\frac{1+\beta_b^2}{1-\beta_b^2}\,\frac{\omega_{pe}^2}{c^2}\,\frac{1}{\left[1+\omega_{ce}^2/\omega_{pe}^2\right]}\right)^{1/2}, \tag{A10}$$

and the longitudinal component of the wave phase velocity is defined by

$$\tilde{V}_{ph}^z = \frac{\tilde{\omega}_{wh}}{k_z} = \frac{k_x\omega_c}{\sqrt{\left[k_x^2+\omega_{pe}^2/c^2\right]\left[k_x^2\left(1+\omega_{ce}^2/\omega_{pe}^2\right)+\omega_{pe}^2/c^2\right]}}. \tag{A11}$$

Similarly, repeating the analysis performed in Sec. V, after some straightforward algebra one can demonstrate that for a non-relativistic beam, $\beta_b << 1$, with $r_b\tilde{k}_{qs} >> 1$, the total wave-field contribution to the transverse component of the Lorentz force vanishes, and the transverse force produced by the local field perturbation is still determined by Eq. (22), i.e.,

$$F_x = Z_b^2 m_e v_b^2\,\frac{1}{n_p}\,\frac{dn_b}{dx}. \tag{A12}$$

APPENDIX B: AXIAL MAGNETIC FIELD PERTURBATION AND LOCAL DIAMAGNETIC PLASMA RESPONSE FOR $\alpha = \omega_{ce}/2\beta_b\omega_{pe} >> 1$

Making use of Eq. (1), after some straightforward algebra we find that the longitudinal component of the magnetic field perturbation is given by $B_z = B_z^W + B_z^{loc}$, where the local component, B_z^{loc}, and the wave component, B_z^W, are specified for $0 < x << l_b^2 \tilde{k}_{em,qs}$ by

$$\frac{eB_z^W}{m_e\omega_{pe}c} = \frac{2\pi Z_b \omega_{ce}\omega_{pe}}{n_p\left(\tilde{k}_{qs}^2 - \tilde{k}_{em}^2\right)}\left(b_z^w + b_z^{qs}\right), \tag{B1}$$

$$b_z^{em,qs} = \left[\tilde{k}_{em,qs}\Big/\left(1+\omega_c^2/\omega_p^2\right)\right]\int_0^\infty dk_z n_{\mathbf{k}}\left(\tilde{k}_{em,qs}, k_z\right)\sin\left(k_z z \pm \tilde{k}_{em,qs}x\right), \tag{B2}$$

$$\frac{eB_z^{loc}}{m_e\omega_{pe}c} = \int_{-\infty}^{\infty} dk_z e^{ik_z\xi}\int_C dk_x e^{ik_x x} n_{\mathbf{k}}\,\frac{Z_b k_x^2 \omega_{ce}\omega_{pe}\Big/\left(1+\omega_{ce}^2/\omega_{pe}^2\right)}{c^2 n_p\left(k_x^2 - \tilde{k}_{em}^2\right)\left(k_x^2 - \tilde{k}_{qs}^2\right)}. \tag{B3}$$

It follows for the case of a nonrelativistic beam, β_b<<1, propagating through a background plasma with $\alpha = \omega_{ce}/2\beta_b\omega_{pe} >> 1$, that the local *z*-component of the magnetic field perturbation is much greater than the wave-field *z*-component, and is given approximately by

$$\frac{eB_z^{loc}}{m_e\omega_{pe}c} \approx -\frac{Z_b\beta_b^2\omega_{pe}}{\omega_{ce}n_p} n_b(x,z), \tag{B4}$$

provided the beam radius r_b satisfies $\tilde{k}_{qs}^{-1} << r_b << \tilde{k}_{em}^{-1}$, or equivalently, $c\left(1+\omega_c^2/\omega_p^2\right)\Big/\left(2\alpha\omega_{pe}\right) << r_b << 2\alpha c/\omega_{pe}$ in the limit $\alpha >> 1$. Equation (B4) demonstrates the diamagnetic plasma response, in accordance with the results obtained in the numerical simulations.

For the critical case where $\alpha = \omega_{ce}/2\beta_b\omega_{pe} \approx 1$, assuming a nonrelativistic ion beam, $\beta_b << 1$, after some straightforward algebra it follows from Eqs. (B1)-(B2) that $\Delta\alpha \equiv \left(eB_z/m_e c\right)\Big/\left(2\beta_b\omega_{pe}\right)$ can be estimated by

$$\Delta\alpha \sim Z_b\left(n_b/n_p\right)\left(r_b\omega_{pe}/c\right)\left[\left(1+\Delta\alpha^2\right)-1\right]^{-1/2}, \tag{B5}$$

provided the beam radius is of the order of or smaller than the electron skin depth. Note that in obtaining Eq. (B5), we have used the fact that $\omega_{ce} << \omega_{pe}$, which is required by the resonance condition, $\alpha = \omega_{ce}/2\beta_b\omega_{pe} = 1$, for the case of a nonrelativistic ion beam pulse.

AKNOWLEDGEMENTS

This research was supported by the U.S. Department of Energy.

[1] P. Chen, Phys. Rev. Lett. **54**, 693 (1985).

[2] C. Joshi, Phys. Plasmas **14**, 055501 (2007).

[3]P. K. Roy, S. S. Yu, E. Henestroza, A. Anders, F. M. Bieniosek, J. Coleman, S. Eylon, W. G. Greenway, M. Leitner, B. G. Logan, W. L. Waldron, D. R. Welch, C. Thoma, A. B. Sefkow, E. P. Gilson, P. C. Efthimion, and R. C. Davidson, Phys. Rev. Lett. **95**, 234801 (2005).

[4] S.S. Yu, R.P. Abbott, R.O. Bangerter, J.J. Barnard, R.J. Briggs, D. Callahan, C.M. Celata, R. Davidson, C.S. Debonnel, S. Eylon, A. Faltens, A. Friedman, D.P. Grote, P. Heitzenroeder, E. Henestroza, I. Kaganovich, J.W. Kwan, J.F. Latkowski, E.P. Lee, B.G. Logan, P.F. Peterson, D. Rose, P.K. Roy, G.-L. Sabbi, P.A. Seidl, W.M. Sharp and D.R. Welch, Nucl. Instr. And Meth. A **544**, 294 (2005).

[5] M. V. Medvedev, M. Fiore, R. A. Fonseca, L. O. Silva, and W. B. Mori, Astrophys. J. Lett. **618**, L75 (2005).

[6] A. Gruzinov, Astrophys. J. Lett. **563**, L15 (2001).

[7]P.A. Seidl, A. Anders, F.M. Bieniosek, J.J. Barnard, J. Calanog, A.X. Chen, R.H. Cohen, J.E. Coleman, M. Dorf, E.P. Gilson, D.P. Grote, J.Y. Jung, M. Leitner, S.M. Lidia, B.G. Logan, P. Ni, P.K. Roy, K. Van den Bogert, W.L. Waldron, and D.R. Welch, Nucl. Instr. and Meth. A **606**, 75 (2009).

[8] A. Friedman, J.J. Barnard, R.J. Briggs, R.C. Davidson, M. Dorf, D.P. Grote, E. Henestroza, E.P. Lee, M.A. Leitner, B.G. Logan, A.B. Sefkow, W.M. Sharp, W.L. Waldron, D.R. Welch, S.S. Yu, Nucl. Instr. and Meth. A **606**, 6 (2009).

[9] R. Lee and R. N. Sudan, Phys. Fluids **14**, 1213 (1971).

[10] K. R. Chu and N. Rostoker, Phys. Fluids **16**, 1472 (1973).

[11] S. E. Rosinskii and V. G. Rukhlin, Sov. Phys. JETP **37**, 436 (1973).

[12] H. L. Berk and L. D. Pearlstein, Phys. Fluids **19**, 1831 (1976).

[13] J. C. Johnson, N. D'Angelo, and R. L. Merlino, IEEE Transactions on Plasma Science **16,** 590 (1988).

[14] I. D. Kaganovich, E. A. Startsev, A. B. Sefkow and R. C. Davidson, Phys. Rev. Lett. **99**, 235002 (2007).

[15] I. D. Kaganovich, E. A. Startsev, A. B. Sefkow and R. C. Davidson, Phys. Plasmas **15**, 103108 (2008).

[16] I. D. Kaganovich, G. Shvets, E. Startsev, and R. C. Davidson, Phys. Plasmas **8**, 4180 (2001).

[17] I. D. Kaganovich, E. Startsev, and R. C. Davidson, Phys. Plasmas **11**, 3546 (2004).

[18] B. V. Oliver, D. D. Ryutov, and R. N. Sudan, Phys. Plasmas **1**, 3383 (1994).

[19] C. Krafft and M. Starodubtsev, Planetary and Space Science **50**, 129 (2002), and references therein.

[20] J. Lavergnat and R. Pellat, J. Geophys. Res. **84**, 12 (1979).

[21] C. Krafft, P. Thévenet, G. Matthieussent, B. Lundin, G. Belmont, B. Lembège, J. Solomon, J. Lavergnat, and T. Lehner, Phys. Rev. Lett. **72**, 649 (1994).

[22] A. Volokitin, C. Krafft, and G. Matthieussent, Phys. Plasmas **2**, 4297 (1995).

[23] A. Volokitin, C. Krafft, and G. Matthieussent, Phys. Plasmas **4**, 4126 (1997).

[24] C. Krafft and A. Volokitin, Phys. of Plasmas **5**, 4243 (1998).

[25] A. I. Ahiezer, I. A. Ahiezer, R. V. Polovin, A. G. Sitenko, and K. N. Stepanov, *Plasma Electrodynamics* (Nauka, Moscow, 1974).

[26] E.A. Startsev, R. C. Davidson and M. Dorf, Phys. Plasmas **15**, 062107 (2008).

[27] LSP is a software product developed by ATK Mission Research, Albuquerque, NM 87110.

[28] I. D. Kaganovich, A. B. Sefkow, E.A. Startsev, R. C. Davidson and D. R. Welch, Nucl. Instr. and Meth. A **577**, 93 (2007).

[29] P. F. Ottinger, Phys. Plasmas **7**, 346 (2000).

[30] K. Hahn and E. Lee, Fusion Engineering and Design **32-33**, 417 (1996).

[31] M. Dorf, I. Kaganovich, E. Startsev and R. Davidson, Phys. Rev. Lett. **103**, 075003 (2009).